

Exp.-Nr. **A2**
Eingang:
an PAC:

Mainz Microtron MAMI

A2 Collaboration at MAMI

Spokespersons: P. Pedroni, A. Thomas

Proposal for an Experiment

”Measurement of the polarization observables T,P,H and F for $p\pi^0$, $n\pi^+$ (and $p\eta$) final states”

Spokespersons for the Experiment :

Farah Afzal (Helmholtz-Institut für Strahlen- und Kernphysik, Bonn, Germany)

Yannick Wunderlich (Helmholtz-Institut für Strahlen- und Kernphysik, Bonn, Germany)

Abstract of Physics :

We propose to simultaneously measure the polarization observables T, P, H and F for neutral and charged pion photoproduction for the incident-photon energy range of $230 \text{ MeV} \leq E_\gamma \leq 830 \text{ MeV}$ to fill existing gaps in the world database. This measurement will allow us to extract model-independently not only the photoproduction multipoles for the individual reactions, but also the isospin multipoles using a truncated partial wave analysis (TPWA) in the region of the $\Delta(1232)_{\frac{3}{2}^+}(P_{33})$, $N(1440)_{\frac{1}{2}^+}(P_{11})$, $N(1520)_{\frac{3}{2}^-}(D_{13})$ and $N(1535)_{\frac{1}{2}^-}(S_{11})$ resonances.

Abstract of Equipment :

The experiment will be performed at the tagged photon facility of MAMI using Crystal Ball/TAPS detector setup together with particle identification detector (PID) and multi-wire proportional chambers (MWPCs).

MAMI Specifications :

beam energy	1557 MeV
beam polarization	longitudinally polarized

Photon Beam Specifications :

tagged energy range	230 – 1448 MeV
photon beam polarization	elliptically polarized (coherent peak positions at 350 MeV, 450 MeV, 550 MeV, 650 MeV, 750 MeV, 850 MeV)

Equipment Specifications :

detectors	Crystal Ball/TAPS, PID, MWPCs, Cherenkov
target	transversely polarized p-butanol target, carbon foam target

Beam Time Request :

time to set-up	24 hours
time to change/pol. target	200 hours
time with beam	930 hours

List of participating authors:

- **Institut für Physik, University of Basel, Switzerland**
D. Ghosal, N. Jermann, B. Krusche, A. Kaeser, C. Meier
- **Institut für Experimentalphysik, University of Bochum, Germany**
G. Reicherz
- **Helmholtz–Institut für Strahlen- und Kernphysik, University of Bonn, Germany**
F. Afzal, R. Beck, A. Thiel, Y. Wunderlich
- **JINR, Dubna, Russia**
N.S. Borisov, I. Gorodnov, A. Lazarev, A. Neganov, Yu.A. Usov
- **SUPA School of Physics and Astronomy, University of Glasgow, UK**
S. Gardner, K. Livingston, I.J.D. MacGregor
- **Racah Institute of Physics, Hebrew University of Jerusalem, Israel**
G. Ron
- **Kent State University, Kent, USA**
D.M. Manley
- **Institut für Kernphysik, University of Mainz, Germany**
P. Achenbach, M. Biroth, F. Cividini, A. Denig, P. Drexler, M.I. Ferretti-Bondy, W. Gradl, L. Heijkenskjöld, V.L. Kashevarov, P.P. Martel, E. Mornacchi, M. Ostrick, V. Sokhoyan, C. Sfienti, M. Thiel, A. Thomas, S. Wagner, J. Wettig
- **University of Massachusetts, Amherst, USA**
R. Miskimen
- **Institute for Nuclear Research, Moscow, Russia**
G. Gurevic
- **INFN Sezione di Pavia, Pavia, Italy**
A. Braghieri, S. Costanza, P. Pedroni
- **Department of Physics, University of Regina, Canada**
G.M. Huber
- **Mount Allison University, Sackville, Canada**
D. Hornidge
- **George Washington University, Washington, USA**
W.J. Briscoe, E.J. Downie, I.I. Strakovsky
- **Department of Physics, University of York, UK**
M. Bashkanov, D.P. Watts, D. Werthmüller
- **Rudjer Boskovic Institute, Zagreb, Croatia**
M. Korolija

1 Motivation

1.1 Complete experiments

Ever since the reaction of pseudoscalar meson photoproduction has been considered a useful tool for baryon spectroscopy, people investigated the problem of so-called *complete experiments* [1, 2]. In its original form, this problem arises from the following situation: the full T -matrix of photoproduction can be decomposed model-independently into 4 so-called spin-amplitudes. These 4 amplitudes are accompanied by a total of 16 polarization observables (see Table 1). Complete experiments are minimal subsets of the 16 observables which are capable of uniquely fixing the 4 amplitudes, up to one overall phase which can depend on energy (E_γ) and scattering angle ($\cos\theta$).

For the problem of the extraction of the full 4 spin-amplitudes, it can be shown mathematically [2] that 8 observables are required at least*. These observables have to be selected carefully and it is seen furthermore that one is forced mathematically to select observables from the double polarization classes which involve recoil polarization, which are however unfortunately very difficult to obtain in an actual measurement.

The complete experiment problem can also be considered in the context of a so-called truncated partial-wave analysis (TPWA). In this scenario, the 4 spin-amplitudes are expanded into a finite number of electric and magnetic photoproduction multipoles $\{E_{\ell\pm}, M_{\ell\pm}\}$, generated via a truncation of the partial wave series at some angular momentum ℓ_{\max} . Then, one tries to extract the multipoles out of the data uniquely, up to one only energy dependent phase.

This problem has been investigated in a recent PhD thesis [3], which built up on previous works [4, 5] and which yielded surprising results: the complete sets in the TPWA generally demand *less* observables than needed for the extraction of the 4 spin-amplitudes and the double polarization observables with recoil polarization can be completely avoided! Under idealized circumstances (vanishing measurement uncertainties, vanishing higher partial waves above ℓ_{\max}), these results are expected to hold for arbitrary truncation orders ℓ_{\max} .

The smallest possible complete sets in the TPWA consist of 4 observables. A list of all complete sets of 4 without recoil polarization is given in Table 2. These complete sets of 4 have been found and tested numerically in a work initiated and completed by Tiator [6].

Table 1: The 16 polarization observables of pseudoscalar meson photoproduction are shown. This Table is a simplified version of the one shown in reference [7].

Beam	Target				Recoil			Target + Recoil			
	-	-	-	-	x'	y'	z'	x'	x'	z'	z'
	-	x	y	z	-	-	-	x	z	x	z
unpolarized	σ_0	T			P			$T_{x'}$	$L_{x'}$	$T_{z'}$	$L_{z'}$
linear	Σ	H	P	G	$O_{x'}$	T	$O_{z'}$				
circular		F		E	$C_{x'}$		$C_{z'}$				

*This result holds only in the academic case where the observables do not have uncertainties.

Another possibility to compose complete experiments in a TPWA is given by the so-called complete sets of 5, which are formed by starting with the four single spin observables $\{\sigma_0, \Sigma, T, P\}$ and adding one additional observable in order to remove all remaining discrete ambiguities [3, 5, 8]. Examples for complete sets of 5 are $\{\sigma_0, \Sigma, T, P, F\}$ or $\{\sigma_0, \Sigma, T, P, G\}$. Contrary to the complete sets of 4, the uniqueness of the TPWA can actually be proven algebraically for the complete sets of 5. The corresponding solution theory is worked out in detail in reference [3].

No matter how one proceeds to form complete experiments in the TPWA, a common feature of the complete sets of 4 and of 5 observables is that they unavoidably require at least one of the polarization observables P and H . When looking at the world database of, for instance, the benchmark-process of π^0 -photoproduction (cf. Figure 4), it becomes directly apparent that there do not exist datasets for P and H with a satisfactory simultaneous kinematic coverage in $(E_\gamma, \cos\theta)$.

1.2 TPWA for pion photoproduction

As an example for the effects of an unsatisfactory measurement of only a single observable, a TPWA published in the PhD thesis [3] will be discussed in the following. In this analysis, data for the process $\gamma p \rightarrow \pi^0 p$ were analyzed in the energy region of the $\Delta(1232)$ resonance, i.e. the low energy region. Data for the complete set $\{\sigma_0, \Sigma, T, P, F\}$ composed of 5 observables have been analyzed and their kinematic coverage is shown in Figure 1. All observables except for the single spin observable P were taken from quite recent MAMI-measurements [9, 10, 12], while for the observable P itself, only the relatively old Kharkov-data [13] were the most recent measurement available.

As can be seen in Figure 1, the Kharkov-data for P are far inferior in statistics compared to the other MAMI-datasets. Therefore, the Kharkov-data represented a 'bottle-neck' for the analysis in two different ways:

- First, a TPWA can only be performed when the employed datasets match exactly on a particular energy bin. In case no exact match is given, some energies of particular angular distributions have to be shifted. In this case, one should always 'bin the analysis down' to the statistically weakest dataset (cf. ref. [7]). Comparing to Figure 1, this means that the TPWA can only be performed on the 7 energy bins dictated by the P -dataset, even though all the other observables have a superior energy binning.

Set-Nr.	Observables			
1	σ_0	Σ	P	F
2	σ_0	Σ	F	H
3	σ_0	T	P	F
4	σ_0	T	P	G
5	σ_0	T	F	H
6	σ_0	T	G	H

Table 2: A list is given for all the possible complete sets of 4 observables in a TPWA, which are formed by using just the single spin and Beam-Target observables. The Table is taken from reference [3].

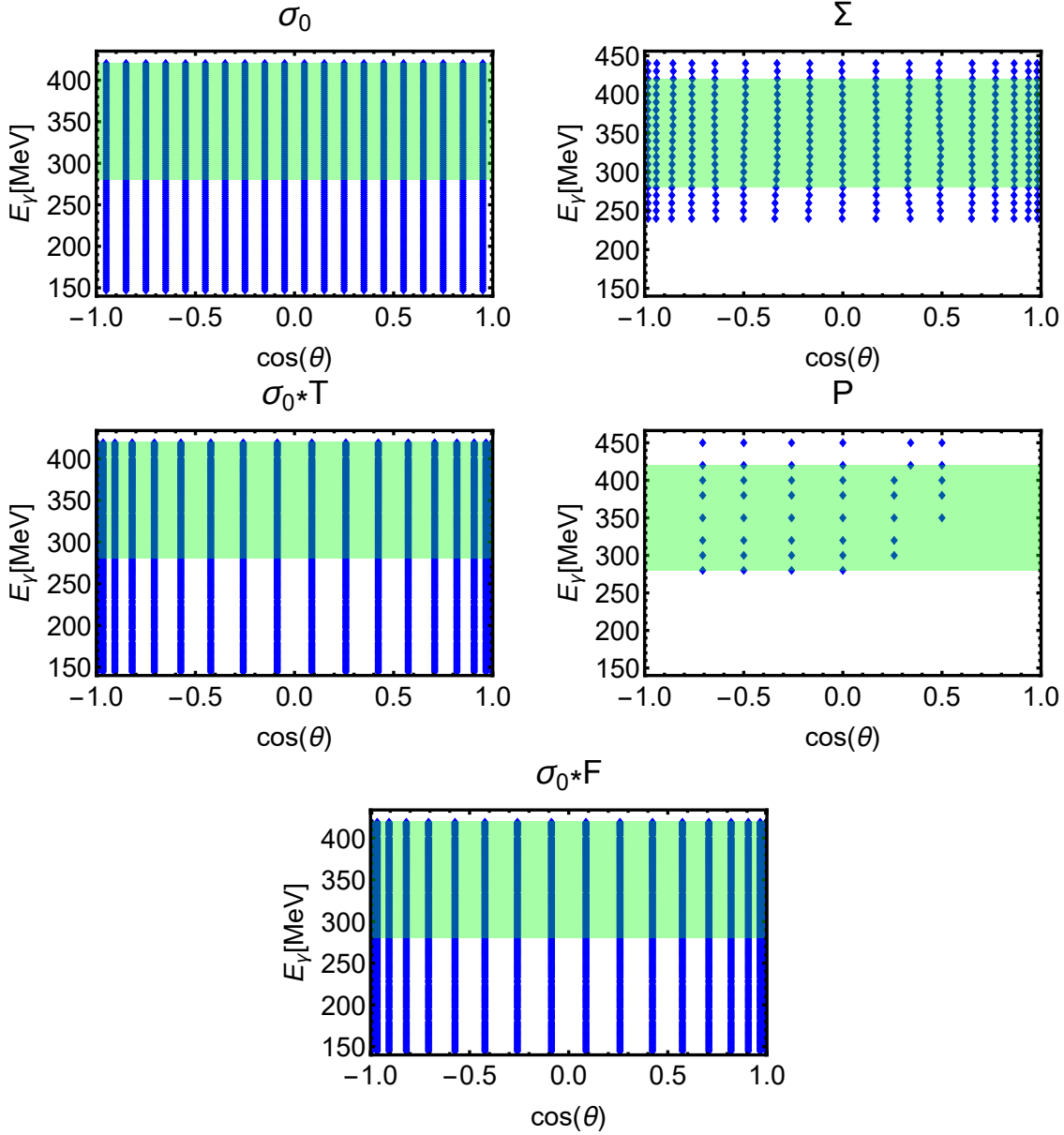


Figure 1: The plots illustrate the kinematical situation for the TPWA in the energy region of the $\Delta(1232)$ resonance, which has been performed for the process $\gamma p \rightarrow \pi^0 p$ in the PhD thesis [3]. The regions in phase space $(E_\gamma, \cos(\theta))$ covered by the datasets for the unpolarized differential cross section σ_0 [9], the dimensionless asymmetries Σ and P [10, 13] and the dimensioned profile functions $\sigma_0 T = \check{T}$ and $\sigma_0 F = \check{F}$ [12] are shown. Blue markers indicate the location of individual datapoints. The green-shaded region illustrates the energy range where all observables overlap, i.e. the area on which the TPWA can be performed. All pictures are taken from [3].

- Second, it is seen in Figure 1 that the angular resolution of the P -dataset is far inferior compared to the MAMI-datasets for the remaining observables and furthermore, the P -data do not cover the extreme angular regions, i.e. data are only given for roughly $|\cos\theta| < 0.75$. A limited angular resolution and, even more importantly, an unsatisfactory angular coverage of the data have been shown to yield sensitive limitations on the precision of Legendre moments extracted from the data [14], which also directly imply severe limitations on the maximal order ℓ_{\max} of uniquely extractable multipoles.

The results of the TPWA in the Δ -region turned out as follows [3]. For the first time, a unique solution for the S - and P -wave multipoles $\{E_{0+}, E_{1+}, M_{1+}, M_{1-}\}$ up to one overall phase has been found, using only the 5 fitted observables and a strict truncation at $\ell_{\max} = 1$. A Monte Carlo-fit method was used which is completely free of any model assumptions. While indeed only one single solution existed for $\ell_{\max} = 1$, the values of χ^2/ndf have been unsatisfactory[†]. Raising the truncation order to $\ell_{\max} = 2$ and again attempting a fully model-independent fit has resulted in multiple possible ambiguous solutions, all with comparable χ^2 , which were undistinguishable based on the data alone. Plotting the angular modulations belonging to the various solutions has made clear that the observable P in particular is missing statistics and angular coverage which is needed to distinguish among the various ambiguities (see Figure 5.51 in ref. [3]). For all the reasons described above, the decision has been made to keep the truncation order at $\ell_{\max} = 2$ but to fix the D -waves to multipoles from the PWA-solution SAID CM12 [15,16]. This again resulted in a unique solution, with improved χ^2 . The results can be seen in Figure 2.

In order to simulate a scenario where the data for P were significantly improved, a further analysis was made in [3] where the Kharkov-data have been exchanged for pseudodata for P which have been generated using the SAID-solution CM12 [16,17]. Starting from the SAID-values for P , pseudodata have been generated with a relative statistical precision of 5%[‡]. Furthermore, the SAID-values had full angular coverage and a very good energy- and angular binning. Using these pseudodata for P , in combination with the real MAMI-data for the remaining 4 observables, all the analysis steps described above have been repeated. Unfortunately, all ambiguities were not removed for the model-independent fit with $\ell_{\max} = 2$, although their overall number has been reduced. Once the D -waves were fixed to SAID, the pseudodata for P still lead to a significant improvement of the statistical uncertainties of the extracted multipoles, as can be seen in Figure 2. Furthermore, the energy-binning of the whole analysis was now adjusted to the Σ -measurement, since the P -data were not setting any limits in that regard any more. This resulted in a much finer binning for the TPWA-results.

Although the improvements brought by the simulated P -dataset were significant, it was not possible to resolve all ambiguities for $\ell_{\max} = 2$. However, there is reason to believe that this will be the case once the 5 observables fitted in this example are enlarged to a set which contains 7 to 8 of all the single spin and Beam-Target observables. This claim is substantiated by another analysis contained in the thesis [3], where the 7 observables $\{\sigma_0, \Sigma, T, P, E, G, H\}$ were analyzed in a slightly higher energy region.

[†]This fact has been traced back, within the thesis [3], to problems with the dataset for the differential cross section. However, this is not relevant for the argument here.

[‡]The algorithmic method to generate the uncertainties for the pseudodata is described in more detail in section 5.5 of the PhD thesis [3].

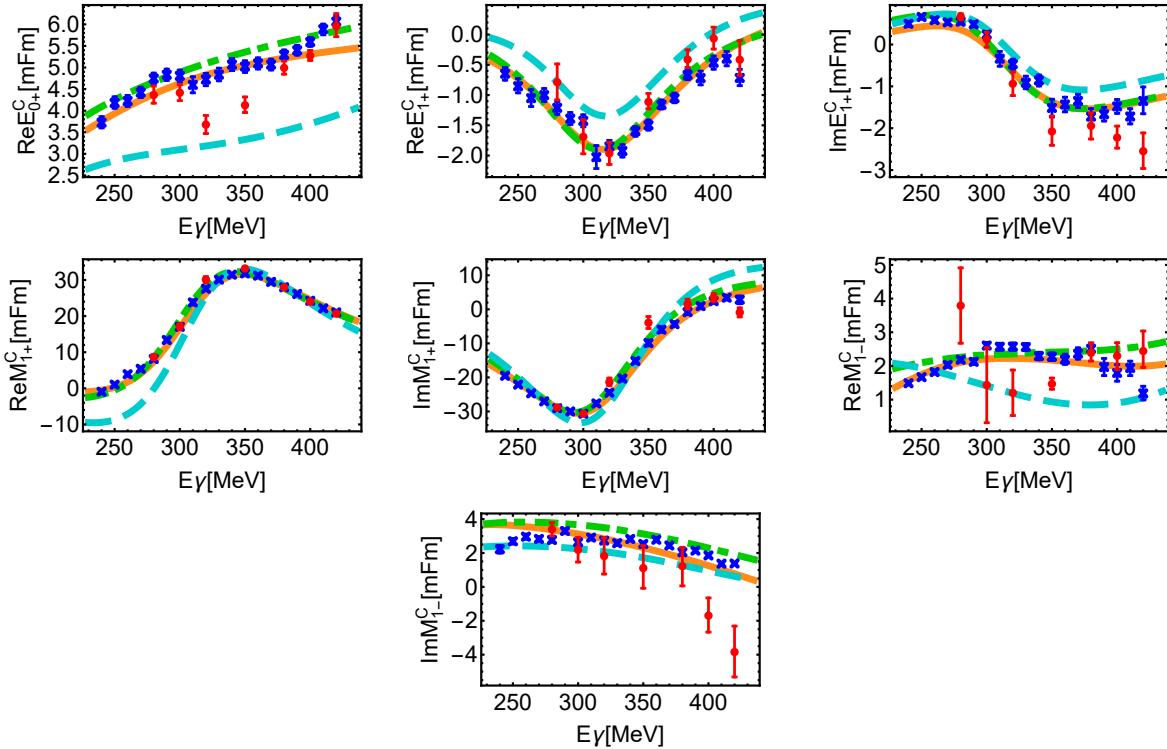


Figure 2: The figures show a comparison of the results of the TPWA in the Δ -region to energy-dependent PWA-models (cf. ref. [3]). Shown are two fits using $\ell_{\max} = 2$, with D -waves fixed to the SAID-solution CM12 [15, 16]. The two sets of symbols indicate two different data-scenarios. A fit to only real measured data for the five observables $\{\sigma_0, \Sigma, T, P, F\}$ (cf. Figure 1) is shown (red dots), as well as a fit to a combination of real data for $\{\sigma_0, \Sigma, T, F\}$ and SAID-pseudodata for P (blue crosses). The SAID-pseudodata have been generated with 5%-uncertainties. Error-bars show statistical uncertainties determined using the bootstrap [3, 18]. The super-script 'C' on the multipoles indicates the fact that the following phase-convention has been used: $\text{Re}[E_{0+}] > 0$ & $\text{Im}[E_{0+}] = 0$. The results of the TPWA are compared to the PWA-solutions SAID CM12 (orange solid line) [16], BnGa 2014.02 (cyan dashed line) [19] and MAID2007 (green dash-dotted line) [20]. All pictures have been taken over identically from reference [3].

In this case, it was possible to find a relatively well-separated global minimum in the fully model-independent fit for $\ell_{\max} = 2$, with not very many ambiguities.

Concerning the process of π^+ -photoproduction ($\gamma p \rightarrow \pi^+ n$), the situation is slightly different compared to the case of π^0 . Here, the pole-term corresponding to pion-exchange in the t -channel is known to dominate at low energies and it has been demonstrated to lead to relatively large values for the higher partial waves [4, 11]. However, as Grushin has demonstrated [4], this apparent disadvantage can be turned into an advantage by parameterizing the pion-exchange using phenomenological Born-terms[§]. Fixing the higher partial waves to the Born-terms then not only resolves the overall-phase ambiguity for the multipoles but can also help with the resolution of further discrete ambiguities. Thus, even though the process of π^+ -photoproduction generally requires the inclusion of higher partial waves, using the Born-terms it becomes even easier to analyze than

[§]These Born-terms are well-known and may be considered as quasi model-independent.

π^0 -photoproduction. Thus, any combination of observables capable of yielding a unique solution for π^0 -photoproduction can also be expected to yield a unique multipole-solution for π^+ -photoproduction. However, for π^+ -photoproduction the kinematic coverage in the low-energy region is equally scarce, which can be seen by inspection of the world database shown in Figure 5.

1.3 Isospin multipoles and direct fit using additional constraints

The TPWA under complete experiment conditions in each reaction individually will, once performed, yield the final sought-after goal of this proposal: multipoles in the isospin-basis. For pion-photoproduction, multipoles corresponding to a particular final state with definite total isospin quantum number $I = 1/2$ or $3/2$ are connected to the individual reaction-multipoles as follows [4, 11]:

$$\mathcal{M}_{\ell\pm}^{(1/2)} = \frac{1}{3} \left(\mathcal{M}_{\ell\pm}^{\pi^0 p} + \sqrt{2} \mathcal{M}_{\ell\pm}^{\pi^+ n} \right), \quad (1)$$

$$\mathcal{M}_{\ell\pm}^{(3/2)} = \mathcal{M}_{\ell\pm}^{\pi^0 p} - \frac{1}{\sqrt{2}} \mathcal{M}_{\ell\pm}^{\pi^+ n}, \quad (2)$$

where $\mathcal{M}_{\ell\pm}^{(I)}$ denotes a generic electric or magnetic isospin multipole $\{E_{\ell\pm}^{(I)}, M_{\ell\pm}^{(I)}\}$. Only with the multipoles in the isospin-basis, it is possible to access all relevant quantum numbers of intermediate resonances.

Instead of first analysing each reaction independently and then reconstructing the isospin multipoles via (1) and (2), one can also try to directly fit the isospin multipoles $\mathcal{M}_{\ell\pm}^{(I)}$ out of the data for both reactions simultaneously. This will be made possible by the proposed beamtime, since the kinematic coverage and binning for all observables is expected to be compatible, for *both* $\gamma p \rightarrow \pi^0 p$ and $\gamma p \rightarrow \pi^+ n$ (see section 1.4 further below). This idea has been explored by Grushin [4] and for the low-energy region, one can exploit further physical constraints:

- For the lowest energies where only the γN - and πN -channels are open, unitarity implies the following relation known as the Fermi-Watson theorem [21]:

$$\mathcal{M}_{\ell\pm}^{(I)} = \left| \mathcal{M}_{\ell\pm}^{(I)} \right| e^{\delta_{I,J}}. \quad (3)$$

Here, $\delta_{I,J}$ is a Pion-Nucleon scattering phase shift with total isospin I and angular momentum J . The idea is now to introduce the equation (3) as a hard constraint into the fit, taking the Pion-Nucleon phases from a known analysis, for instance SAID [16], and then varying the moduli $\left| \mathcal{M}_{\ell\pm}^{(I)} \right|$ as free parameters.

However, the problem here is that the Fermi-Watson theorem is strictly valid only up to the $\pi\pi N$ -threshold, i.e. up to $W_{\pi\pi N} = \sqrt{s_{\pi\pi N}} = m_N + 2m_\pi = 1211 \text{ MeV}$, or $E_\gamma^{\pi\pi N} = 311.4 \text{ MeV}$. Using the Watson-theorem in such a strict way has in the past already lead to unique solutions for very small data-bases (see [11]). Thus, it is anticipated to work and yield even better results with the newly proposed data.

- In order to extend the applicability of the Watson-theorem, one has to use the knowledge gained in phenomenological Pion-Nucleon analyses [16], which states

that certain Pion-Nucleon- phases remain elastic in a good approximation up to intermediate energies, i.e. up to around $E_\gamma = 500\text{MeV}$ to 550MeV . One example for such a phase would be the P_{33} -phase, i.e. $\delta_{3/2,3/2}$.

Using this phenomenologically extended version of the Fermi-Watson theorem up to the intermediate energies, one can fit the isospin multipoles, but using the following constraints only for the E_{1+} - and M_{1+} -multipoles:

$$E_{1+}^{(3/2)} = \left| E_{1+}^{(3/2)} \right| e^{\delta_{3/2,3/2}}, \quad (4)$$

$$M_{1+}^{(3/2)} = \left| M_{1+}^{(3/2)} \right| e^{\delta_{3/2,3/2}}. \quad (5)$$

In the fit, the moduli of these two multipoles, as well as the real- and imaginary parts of all the remaining isospin multipoles, have to be extracted. Using the proposed new data, we again expect very good results using this slightly relaxed constraint.

- Another idea, which Grushin actually mainly pursued in his work [4], was to demand equality for the phases of electric and magnetic multipoles of the same quantum numbers. For instance, he demanded the following constraints:

$$\delta_{E_{1+}^{(3/2)}} = \delta_{M_{1+}^{(3/2)}}, \quad (6)$$

$$\delta_{E_{1+}^{(1/2)}} = \delta_{M_{1+}^{(1/2)}}. \quad (7)$$

On a first glance, this does not look any different from the Fermi-Watson theorem. However, one has to note that only the equality of phases was demanded, but nowhere was it asked that these have to be Pion-Nucleon phases.

Using the third constraint of the equality of the phases, Grushin was able to deduce a unique multipole-solution in the isospin-basis, which can be inspected in Figure 7 of appendix A. However, note that Grushin used only a limited database including measurements of rather poor quality. His π^0 - and π^+ -databases each consisted of measurements for the four single spin observables $\{\sigma_0, \Sigma, T, P\}$, compiled from a list of references which have all been published most of the times well before 1983 (see the paper [4] and references therein). Furthermore, he had to introduce further assumptions to resolve ambiguities and thus arrive at the solution shown in Figure 7. Therefore, with the data taken in the proposed beamtime, we expect to improve on these results significantly, and we expect to be able to extract isospin multipoles for the first time in a maximally model-independent way.

The new isospin multipoles will represent a new benchmark in model-independent TPWAs. They will serve as an ideal testing-ground for the results of the energy-dependent PWAs [16, 19, 20], as well as other phenomenological analysis schemes (see, for instance, the method using fixed- t analyticity by the Mainz/Tuzla-collaboration [22]). Furthermore, the new isospin multipoles can also be used in order to determine the pole-positions of resonances, for instance by using the newly established Laurent+Pietarinen-expansion method [23].

1.4 Existing database and proposed measurements

The kinematic coverage of the data existing in the world database is shown for π^0 -photoproduction in Figure 4 and for π^+ -production in Figure 5. In each case, plots are

shown for the 8 observables comprising all measurements of the single spin- and Beam-Target-classes, i.e. for $\{\sigma_0, \Sigma, T, P, E, G, H, F\}$. The data shown in both plots also contain measurements from two recent PhD-theses [24, 25]. As argued above, these 8 observables are crucial for the complete experiment in a TPWA.

In the case of π^0 -photoproduction, it is seen that for the 4 observables $\{\sigma_0, \Sigma, E, G\}$, measurements exist with good coverage of the full angular region. Data are present for all energies from near threshold up to, for most observables, the very high energies, i.e. around $E_\gamma \simeq 1600\text{MeV}$. Only for the observable G , data with acceptable angular coverage run out at roughly $E_\gamma \simeq 1300\text{MeV}$. For the observables $\{T, P, F, H\}$ and especially in the lower energy region, data are either scarce or non-existent. This is especially true for the observables P and H , where some CBELSA/TAPS-data exist with acceptable angular coverage within the energy region from $E_\gamma \simeq 700\text{MeV}$ to $E_\gamma \simeq 900\text{MeV}$. Outside of this window, good data for P and H are practically non-existent. For T and F , very good threshold-measurements exist up to $E_\gamma = 400\text{MeV}$, but for all existing datasets above this energy, the angular coverage and resolution should be improved. Still, the observables P and H are most important for the complete experiment in the TPWA and here the π^0 -database definitely needs improvement.

For π^+ -photoproduction, the data are generally more scarce than for π^0 . In the low-energy region, i.e. from threshold up to $E_\gamma \simeq 800\text{MeV}$, there exist acceptable datasets for the four observables $\{\sigma_0, \Sigma, E, G\}$. In the case of Σ however, there is still a small gap between $E_\gamma = 450\text{MeV}$ and 570MeV where the angular region is not covered fully. However, this gap is relatively small. The most problems in case of π^+ -photoproduction can again be seen for the four observables $\{T, P, F, H\}$. Here, there are either no data at all (F), or there exist datasets which have big gaps in the angular distributions (T , P and H), where sometimes not even half of the angular range is covered. New data for the $n\pi^+$ final state is expected from the CLAS collaboration. However, they have taken data with six different coherent edge settings at 900 MeV, 1100 MeV, 1300 MeV, 1500 MeV, 1700 MeV and 1900 MeV, which will cover the energy range from 725 MeV - 1875 MeV [26]. Thus, there will be only little overlap between the CLAS data and the data from the proposed experiment.

At this point, the proposed measurement is aimed specifically at filling up the above-mentioned gaps in the world database for both of the processes $\gamma p \rightarrow \pi^0 p$ and $\gamma p \rightarrow \pi^+ n$ within a single measurement period. The goal is to record data that allow for a simultaneous extraction of the observables $\{T, P, F, H\}$ from near threshold up to $E_\gamma \simeq 830\text{MeV}$. As already elaborated above, these measurements indeed close all the relevant gaps in the simultaneous kinematic coverage of polarization measurements of both π^0 - and π^+ -photoproduction in the low-energy region. As a result, one would obtain all 8 observables from the classes of single spin- and Beam-Target measurements in a common energy-binning of at least $\Delta E_\gamma \simeq 34\text{MeV}$ and with fully angular coverage and good angular resolution (We aim at 18 equidistant angular points over the region $\cos\theta \in [-0.95, 0.95]$.). The beamtime estimation given in section 3 gives further insights into how such a kinematic binning can be achieved. In addition, we aim to take data with resulting statistical uncertainties of 5% for all four polarization observables just like for the SAID pseudodata for P .

The proposed method of measurement has already been tested in the recent PhD thesis [24] and it uses elliptically polarized photons impinged on a transversely polarized target. The general expression for the polarized differential photoproduction cross section

reads (cf. expressions in references [7, 27])

$$\left(\frac{d\sigma}{d\Omega}\right)^{(B,T)}(\vec{\epsilon}, \vec{P}^T) = \sigma_0 \left\{ 1 - \Sigma \epsilon_L \cos(2\varphi) + P_x^T [F \epsilon_c + H \epsilon_L \sin(2\varphi)] \right. \\ \left. + P_y^T [T - P \epsilon_L \cos(2\varphi)] \right\}, \quad (8)$$

where $\vec{\epsilon}$ is the polarization vector with the linear ϵ_L and the circular polarization ϵ_c component, P_x^T and P_y^T the target polarization degree in transverse direction and φ is the azimuthal angle between the beam polarization vector and the reaction plane. One can indeed see that under the proposed polarization configuration, the four observables $\{T, P, H, F\}$ can be accessed simultaneously.

All arguments made above serve to illustrate that with these new data, multipole analysis (i.e. TPWA) can be performed in both reactions individually under complete experiment conditions. By this, one can expect a unique extraction of all multipoles up to and including (at least) the D -waves without any model assumptions. For π^+ -photoproduction, one can expect to infer information on higher partial waves up to the F - and G -waves from the data, which however will be fixed to the Born-terms.

In addition, we intend to use the proposed beamtime to also extract the observables T, P, H and F for the $p\eta$ final state. In particular, we want to recheck the results of already published T and F data [28] since the CBELSA/TAPS collaboration reported systematic discrepancies of a factor of 1.40 ± 0.05 to the A2 data [29]. This currently causes problems for partial wave analysis groups, as it is not clear which data sets to take into the fitted database.

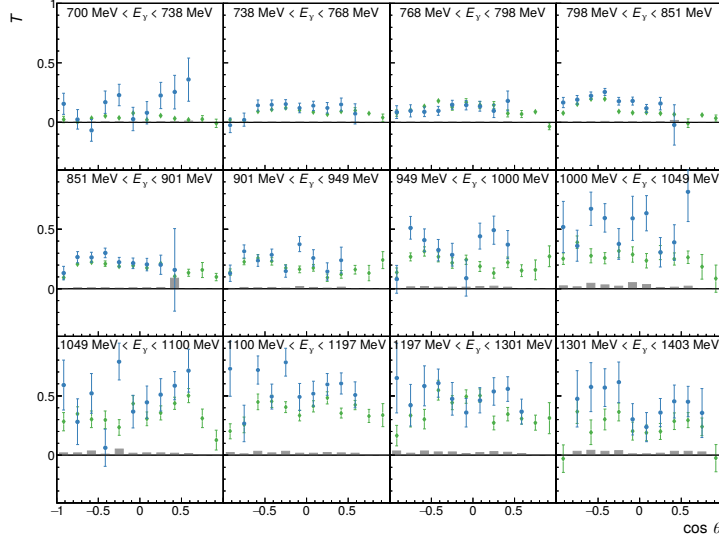


Figure 3: The polarization observable T is shown as a function of $\cos \theta_\eta$ for several energy bins. The blue points are CBELSA/TAPS data [29] and the green points are A2 data [28]. definite isospinTaken from [29].

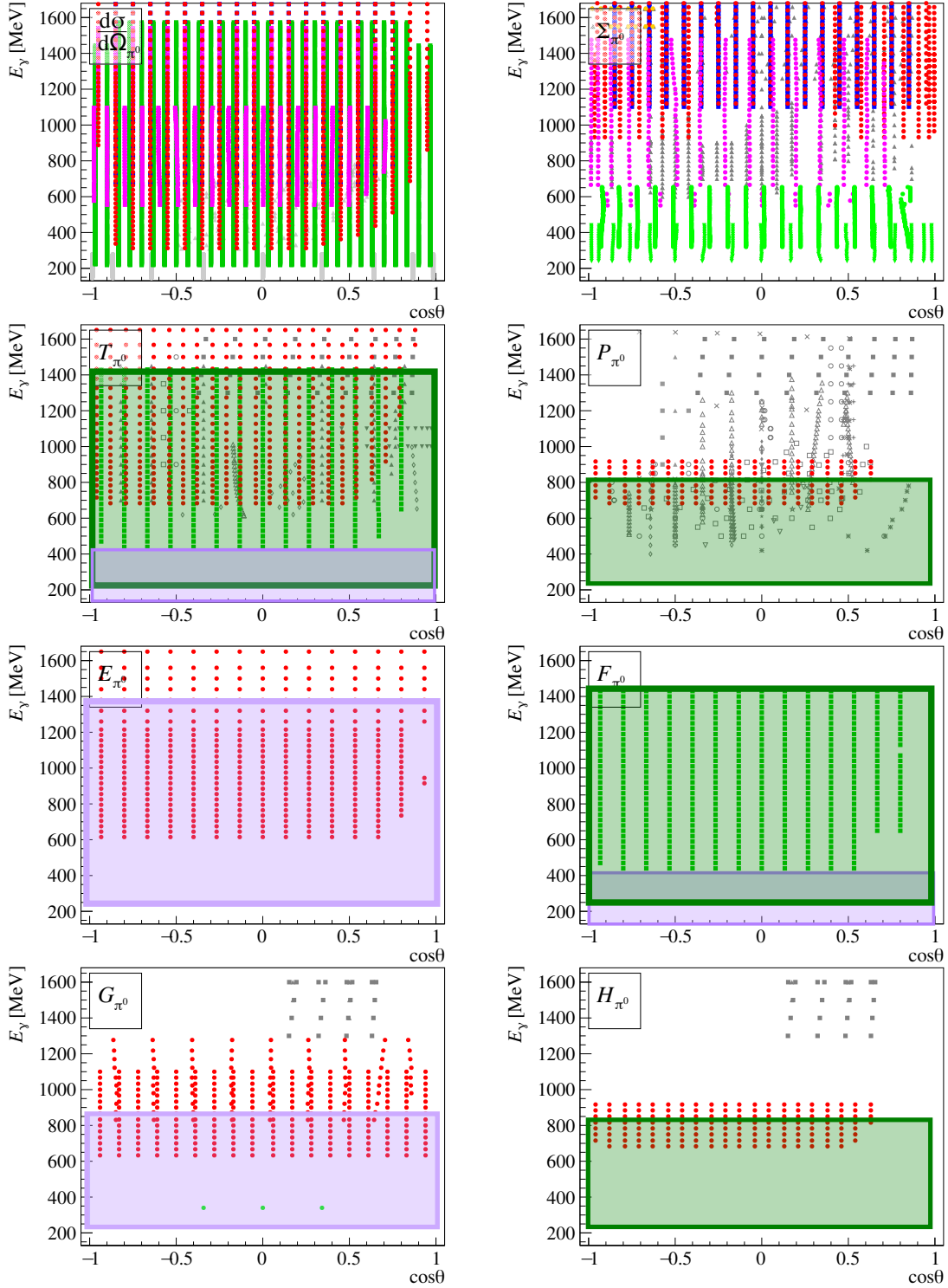


Figure 4: The existing database of the polarization observables T , P , H and F is shown for the $p\pi^0$ final state. The green points represent A2 data, the red points CBELSA/TAPS data, and the gray points represent data sets prior to 2005. The violet boxes show the kinematic range of partially published (T , F) or soon to be published (G , E) A2 data. The green boxes show the energy and angular range that will be covered by the proposed experiment. The references of all data sets can be found in [24, 25].

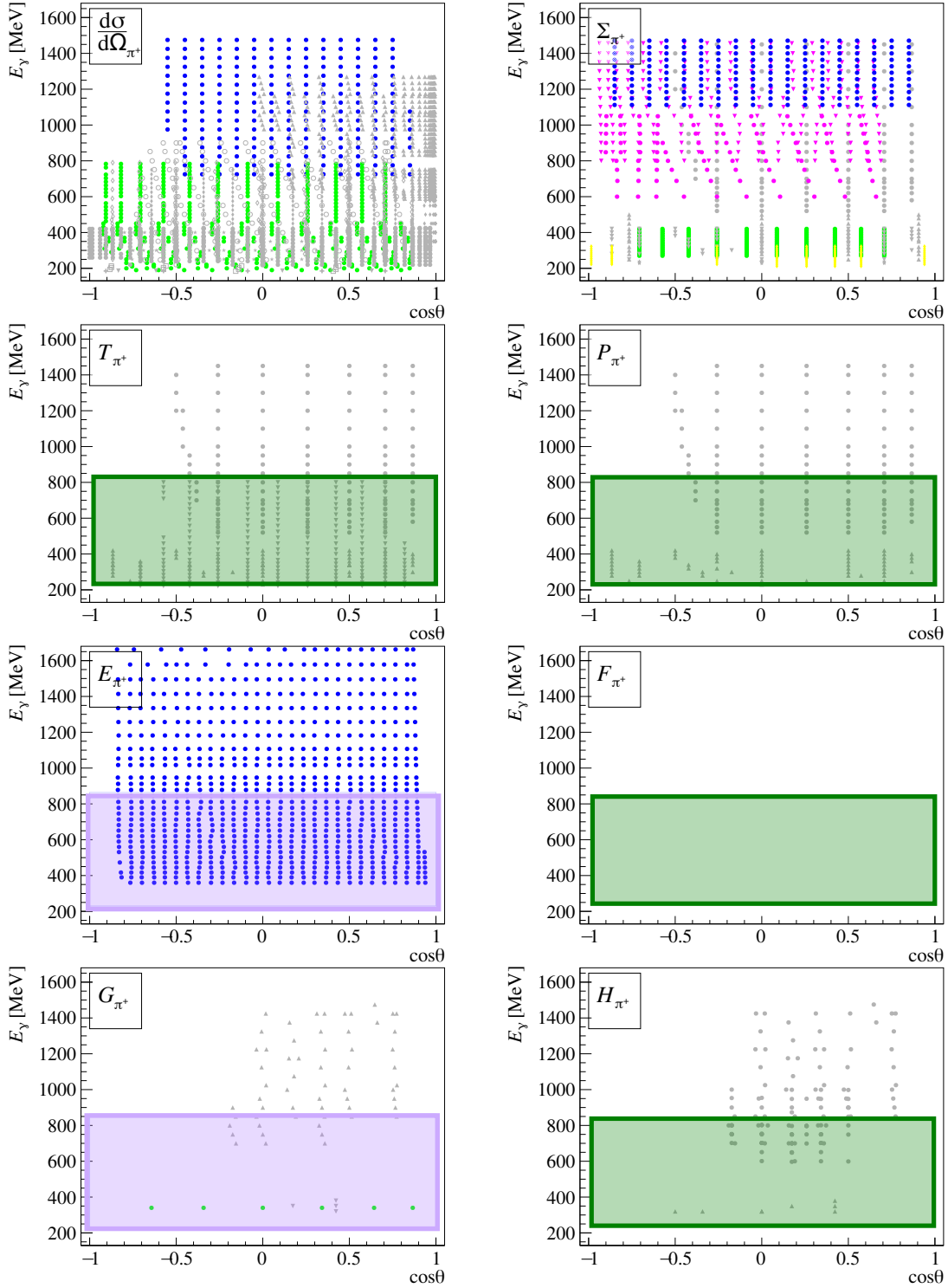


Figure 5: The existing database of the polarization observables T , P , H and F is shown for the $n\pi^+$ final state. The green points represent A2 data, the red points CBELSA/TAPS data, the blue points CLAS data and the gray points represent data sets prior to 2005. The violet boxes show the kinematic range of soon to be published (G , E) A2 data. The green boxes show the energy and angular range that will be covered by the proposed experiment. The references of all data sets can be found in [25].

2 Experiment

We propose to measure the polarization observables T , P , H and F within a single beam-time for the $p\pi^0$ and $n\pi^+$ final states for an incident photon beam energy range of $230 \text{ MeV} \leq E_\gamma \leq 830 \text{ MeV}$. While the polarization observables P and H require a linearly polarized photon beam, the polarization observable F needs a circularly polarized photon beam. To measure all observables simultaneously as proposed, an elliptically polarized photon beam with a linear and circular polarization component will be used. In addition, a transversely polarized frozen-spin butanol target is needed for all four observables (see Table 1).

2.1 Photon beam

The electron beam provided by the MAMI accelerator can impinge on a radiator, producing Bremsstrahlung photons. These photons can be either linearly polarized if an unpolarized electron beam is used on a crystalline radiator, or they can be circularly polarized if longitudinally polarized electrons are used on an amorphous radiator. The elliptically polarized photon beam will be produced using longitudinally polarized electrons that will be incident on a diamond crystal radiator of $100 \mu\text{m}$ thickness. The measurement will be performed with a MAMI-C beam energy of $E_0 = 1557 \text{ MeV}$ to achieve high polarization degree values for the linear polarization component. The polarization degree can be increased by using a narrow collimator of e.g. 2 mm diameter. To cover the energy range from 230 MeV - 830 MeV for the polarization observables P and H , six different coherent edge positions from 350 MeV to 850 MeV in 100 MeV steps are needed. Maximal polarization values p_γ^{lin} for these configurations range from 75% down to 35% (see Figure 8).

The circular polarization degree p_γ^{circ} reaches at maximum $\sim 80\%$ at $E_\gamma = 1448 \text{ MeV}$ and decreases towards low energies down to $\sim 10\%$ at $E_\gamma = 230 \text{ MeV}$, limiting the energy range of interest for F between $E_\gamma = 230 \text{ MeV}$ and $E_\gamma = 1448 \text{ MeV}$. The polarization degree p_γ^{circ} depends on the electron polarization degree p_e and the energy ratio E_γ/E_0 (see Figure 8). The electron polarization degree will be determined via regular Mott measurements.

2.1.1 Feasibility of using elliptically polarized photons

Data with an elliptically polarized photon beam were taken from November 2013 - September 2015 at the A2 experiment with the goal to determine the polarization observables G and E simultaneously. The results for the polarization observable E are depicted for two energy bins in Figure 6.

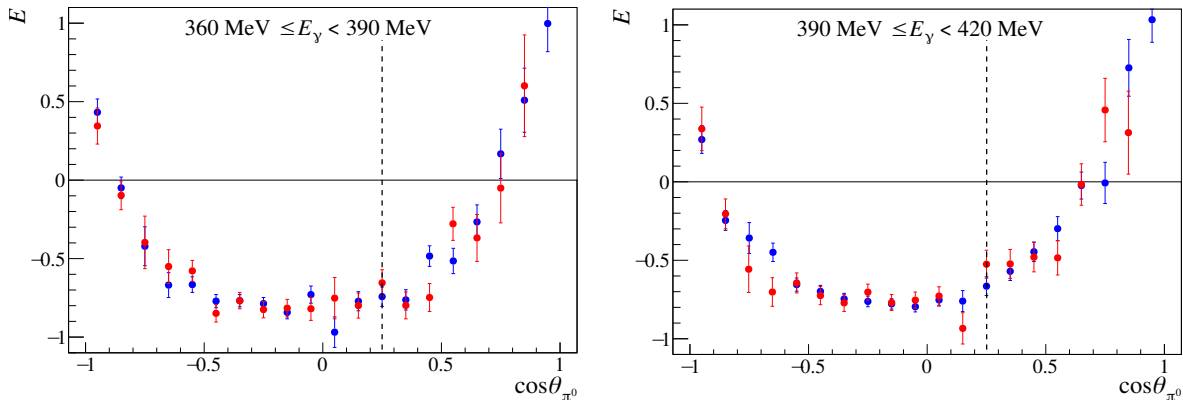


Figure 6: The double polarization observables E is shown for two energy bins as a function of $\cos\theta_{\pi^0}$ for the $p\pi^0$ final state. The data were taken once with a diamond radiator with a coherent edge position of 450 MeV (blue), resulting in elliptically polarized photons and once with an amorphous radiator (red), resulting in only circularly polarized photons. [24]

They are compared to data of the same beamtime where the diamond crystal was exchanged by an amorphous radiator, thus producing only circularly polarized photons. Both results are well in agreement, demonstrating that polarization observables requiring a circularly polarized photon beam can be measured with an elliptically polarized photon beam [24]. The polarization observable G that requires linearly polarized photons, was extracted as well and good agreement was found to existing data from the CBELSA/TAPS collaboration [25].

2.1.2 Photon flux

The required tagged photon energy range is $E_\gamma = 230 \text{ MeV} - 1448 \text{ MeV}$. Figure 10 shows the expected electron rates \dot{N}_{e^-} in MHz per MeV for the MAMI-C beam energy of 1557 MeV, assuming the first tagger channel is run at 2.5 MHz and a $1/E_\gamma$ Bremsstrahlung distribution. Switching off the first 25 tagger channels will allow us to focus on the desired energy range and to increase the rates therein. Using a collimator with a diameter of 2 mm will result in a tagging efficiency of $\epsilon_{\text{tagg}} \approx 27\%$ (see Table 4). The expected photon flux $\dot{N}_\gamma(\Delta E)$ for a certain energy range ΔE is given by

$$\dot{N}_\gamma(\Delta E) = \dot{N}_{e^-}(\Delta E) \cdot \epsilon_{\text{tagg}}. \quad (9)$$

2.2 Frozen-spin butanol target

Apart from a polarized photon beam, the proposed measurement requires a transversely polarized target. Here, a frozen-spin butanol ($\text{C}_4\text{H}_9\text{OH}$) target will be used. The butanol target will be placed in a $^3\text{He}/^4\text{He}$ dilution cryostat which can be operated at approximately 27 mK. The hydrogen nuclei of butanol are polarizable with a maximum polarization degree of $p_T \approx 90\%$ and an average polarization degree of $p_T \approx 70\%$. To account for the unpolarized background contributions stemming from the bound carbon, oxygen and helium nuclei, measurements need to be performed with a carbon foam target as well. The target area densities are expected to be $n_{T,H} = 0.092 \text{ barn}^{-1}$ for the free,

polarizable hydrogen protons of the butanol target, $n_{T,B} = 0.68 \text{ barn}^{-1}$ for the total butanol target and $n_{T,C} = 0.6 \text{ barn}^{-1}$ for the carbon target[¶]. More details about the target can be found in appendix B.2.

2.3 Detector equipment, detection and reconstruction efficiencies

Both mesons, the π^0 and the η decay to two photons. Therefore, we propose to use the Crystal Ball and the TAPS calorimeters (see Figure 12), which are ideally suited to detect the decay photons in the polar angular range of $1^\circ \leq \theta_{\text{lab}} \leq 159^\circ$ and thus, enable the reconstruction of the π^0 and the η mesons in the final state. The detection of the proton in addition helps to reduce background contributions. The detection and reconstruction efficiency ϵ_{acc} is on average $\sim 75\%$ for $p\pi^0$ (see Figure 16) and $\sim 50\%$ for $p\eta$, respectively. Figure 13 shows a typical two photon invariant mass spectrum from previously taken data. The $p\pi^0$ and $p\eta$ final state can be selected well with low background contributions of $< 2\%$ and $< 6\%$ over almost the complete energy and angular range, respectively. Furthermore, almost the full azimuthal angular range ϕ is covered by both calorimeters, which is needed for the determination of the polarization observables P and H .

The reconstruction of the $n\pi^+$ final state is more challenging. First of all, the PID, MWPCs and TAPS vetoes are essential for the identification of a charged particle (π^+). In addition, the PID and TAPS vetoes in combination with the calorimeters allow the identification of the charged pions and separate them from protons and electrons/positrons using the $\Delta E - E$ method (see Figure 14). Below $E_\gamma = 450 \text{ MeV}$, the detection of the π^+ alone is sufficient. Here, the detection and reconstruction efficiency is about 30%. However, at higher energies background contributions from channels like $n\pi^+\pi^0$, $p\pi^+\pi^-$ can be only rejected with the additional detection of the neutron according to Monte Carlo simulations. This leads to a reduction of the detection and reconstruction efficiency to $\sim 8\%$ for the $n\pi^+$ final state (see Figure 16). The analysis of the $n\pi^+$ final state is limited to $E_\gamma \leq 1000 \text{ MeV}$ since almost all π^+ are minimum ionizing and punch through the calorimeters above this energy. Figure 21 shows a comparison between the latest A2 data and the CLAS data for the double polarization observable E . The results are in good agreement, demonstrating the feasibility of analyzing the $n\pi^+$ final state.

Besides, a Cherenkov detector that is filled with CO_2 , can be placed between the Crystal Ball and the TAPS calorimeters. Electrons or positrons passing through the Cherenkov detector with an energy higher than approximately 10 MeV will produce Cherenkov light. The Cherenkov detector is needed due to the required trigger configuration (see next section).

2.4 Trigger configuration

The successful extraction of the multipole amplitudes with small uncertainties is only possible if the full polar angular range is covered by the data. Therefore, it is essential

[¶]The target area density of the carbon target will be matched to the contribution of the bound nuclei within the butanol target.

to investigate what the optimal trigger configuration is for the data-taking. The Crystal Ball calorimeter offers the possibility to trigger on the analogue sum of all ADCs, which gives the total deposited energy and which is referred to as the *CB Esum* trigger. Based on MC simulations and previous data, it was found that the $n\pi^+$ final state requires a lower *CB Esum* trigger threshold of ~ 40 MeV than $p\pi^0$ (~ 80 MeV) or $p\eta$ (~ 150 MeV) (see Figure 17-19). Therefore, the overall choice of the trigger configuration is dictated by the $n\pi^+$ final state. In addition, investigations showed that the *CB Esum* trigger alone will not suffice to cover the forward polar angular range ($\cos\theta_{\pi^+} > 0.7$) when the π^+ is detected by the TAPS calorimeter (or when the n is detected in TAPS for $\cos\theta_{\pi^+} < -0.7$). Here, an additional trigger on the deposited energy in the individual BaF₂ elements can be set. The optimal setting of the TAPS LED1 thresholds for the $n\pi^+$ final state are also ~ 40 MeV (see Figure 19). To avoid triggering primarily on electromagnetic background, it is important to ask for a veto from the Cherenkov detector in case of the TAPS trigger.

3 Beamtime request

The required beamtime t_{beam} is estimated for the polarization observables P and H since these two polarization observables can not be analyzed for the full data set, but the data has to be divided into sub-data sets according to the chosen coherent edge setting. However, this restriction does not apply for the polarization T and F , resulting automatically in a better statistical accuracy for T and F than for P and H . In addition, the estimation is carried out for the $n\pi^+$ final state due to its much lower detection and reconstruction efficiency compared to the $p\pi^0$ final state. This difference is larger than the difference between the total cross sections above $E_\gamma = 450$ MeV (see Figure 15).

It is desirable to have an energy binning for the polarization observables that matches at least to the already existing data (e.g. G), which means an energy binning with a width of $\Delta E = 34$ MeV is needed at least. Besides, a good polar angular binning of $N_\theta = 18$ is desirable for a truncation of the TPWA at $\ell_{\text{max}} = 4$ and a statistical accuracy of $\Delta O = 5\%$. The required beamtime is then given by

$$t_{\text{beam}} = N_\theta \left[p_\gamma^2 \cdot p_T^2 \cdot (\Delta O)^2 \cdot \dot{N}_\gamma \cdot n_T \cdot \sigma_{\text{tot}} \cdot \epsilon_{\text{acc}} \cdot \Gamma \cdot f_{\text{lifetime}} \right]^{-1}, \quad (10)$$

with

- p_γ : degree of linear polarization, estimated at the center of each energy bin
- $p_T \sim 70\%$: average target polarization degree
- $\Delta O = 0.05$: statistical precision of observable
- \dot{N}_γ : photon flux for the complete energy bin width (see Eq. 9)
- $n_T = 0.0918$ barn⁻¹: number of free protons in butanol target
- σ_{tot} : total unpolarized cross section (see Figure 15)
- $\epsilon_{\text{acc}} = \begin{cases} 0.3 & E_\gamma \leq 450\text{MeV} \\ 0.08 & E_\gamma > 450\text{MeV} \end{cases}$: average detection and reconstruction efficiency

- $\Gamma = 1$: branching ratio
- $f_{\text{lifetime}} \approx 60\%$

Each coherent edge setting will cover roughly three energy bins. Table 3 gives an overview of the required beamtime per coherent edge setting. Due to the decrease of the linear polarization degree at higher energies, the required time increases for higher coherent edge positions. The carbon target has a much higher target area density compared to the free protons of the butanol target, resulting in a lower required beamtime for the background measurements. Furthermore, Table 3 lists the time of already taken data that was used to extract the polarization observable G (which is comparable to the polarization observables P and H). The achieved statistical accuracy of this previous data is demonstrated in Figure 20 for the $n\pi^+$ final state.

coherent edge [MeV]	time _{butanol} [h]	time _{carbon} [h]	time _G [h]
350	8	1	11
450	18	2	55
550	74	10	20
650	119	16	90
750	147	20	67
850	363	49	92
total	729 h (30 d)	98 h (4 d)	335 h (14 d)

Table 3: This table gives an overview of the required data taking time with beam for each coherent edge setting and for both the butanol and the carbon target as calculated using Eq. 10. In addition, the number of hours are given for the already analyzed data that were used to determine the double polarization observable G . The results for the double polarization observable G for the $n\pi^+$ final state are shown in Figure 20 and give an estimation about the statistical precision that can be achieved within the listed time frame.

In addition, tagging efficiency runs (with low rates for normalization) and Mott measurements need to be performed on a daily basis, that take approximately 3 h per day and 102 h in total. Thus, a total of ~ 930 h are needed with beam. Furthermore, ~ 200 h are estimated for the repolarization of the target, the change of target polarization direction and the change between the butanol and the carbon target.

The expected count rates \dot{N}_π for the $p\pi^0$ and the $n\pi^+$ final states are given by

$$\dot{N}_\pi = \dot{N}_\gamma \cdot n_T \cdot \sigma_{\text{tot}} \cdot \epsilon_{\text{acc}} \cdot \Gamma. \quad (11)$$

For the desired energy range of $230 \text{ MeV} \leq E_\gamma \leq 830 \text{ MeV}$, a count rate of 1367 Hz (185 Hz) is expected for the butanol target (polarizable hydrogen component of butanol) and for the $p\pi^0$ final state. A rate of 303 Hz (41 Hz) is expected for the $n\pi^+$ final state. In previous beamtimes data were taken with a trigger rate of ~ 3 kHz and a livetime of 60%. Thus, we will be able to record all the data we want to have.

In addition, it is expected to have uncertainties in the order of $\sim 10\%$ for the polarization observables of the $p\eta$ final state. This high-statistics data set will enable us to check for systematic effects of the previously published data.

A Grushin's fit of the isospin multipoles

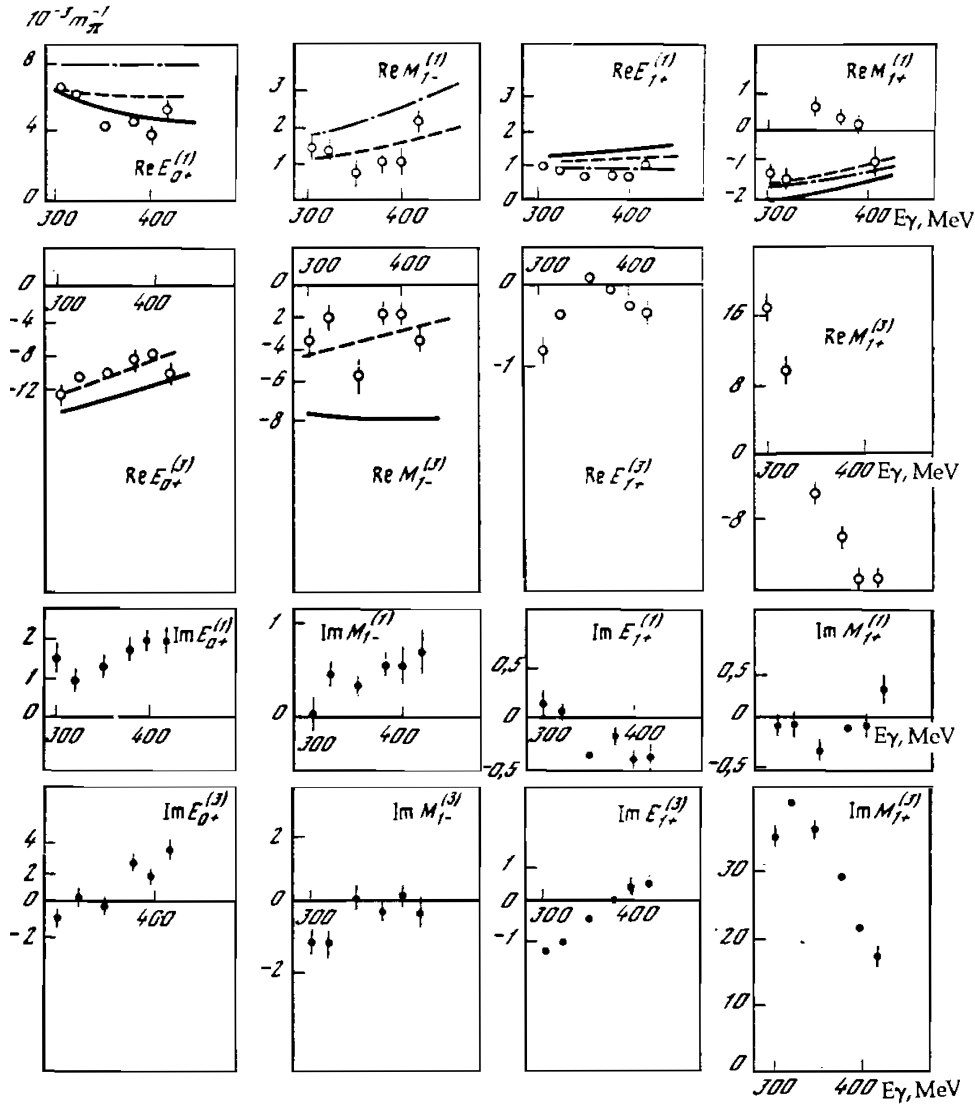


Figure 7: Shown are the results of Grushin's fit [4] for the extraction of isospin-multipoles up to $\ell_{\max} = 1$, performed on 6 energies within the low-energy region of the reactions $\gamma p \rightarrow \pi^0 p$ and $\gamma p \rightarrow \pi^+ n$. Real and imaginary parts of all multipoles for $\ell = 0$ and 1 are shown in units of $10^3 m_\pi$. The original figure has been taken over from reference [4] (cf. Figure 23 on page 85 of that reference).

B Experimental apparatus

B.1 Photon Beam

The A2 photon beam is derived from the production of Bremsstrahlung photons during the passage of the MAMI electron beam through a thin radiator. The resulting photons can be circularly polarised, with the application of a polarised electron beam, or linearly

polarised, in the case of a crystalline radiator. The degree of polarisation achieved is dependent on the energy of the incident electron beam (E_0), the energy range of interest, and in the case of linear polarisation on the photon collimator size. Together, these currently result in a peak of $\sim 75\%$ for linear polarisation (Fig. 8) and $\sim 80\%$ for circular polarisation (Fig. 8). The collimator size, as well as the electron beam energy, also affect the ratio of photons that reach the target to those produced in the Bremsstrahlung process. Typical values for this ratio, denoted as the tagging efficiency, are shown in Tab. 4. The upgraded A2 Photon Tagger (Fig. 9) provides energy tagging of the photons by detecting the post-radiating electrons with a single-counter time resolution $\sigma_t = 0.1$ ns [30]. With the upgrade, individual counters can now operate reliably above 1 MHz, although the loss due to pile-up is $\sim 1.8\%$ per 1 MHz rate. A typical limit of 2.5 MHz is employed to keep the pile-up loss below 5%. Photons can be tagged in the momentum range from 4.3 to 93.0% of E_0 , with resolutions varying from 0.4 to 0.05% of E_0 , respectively. This relationship, along with sample rate distributions, is shown in Fig. 10.

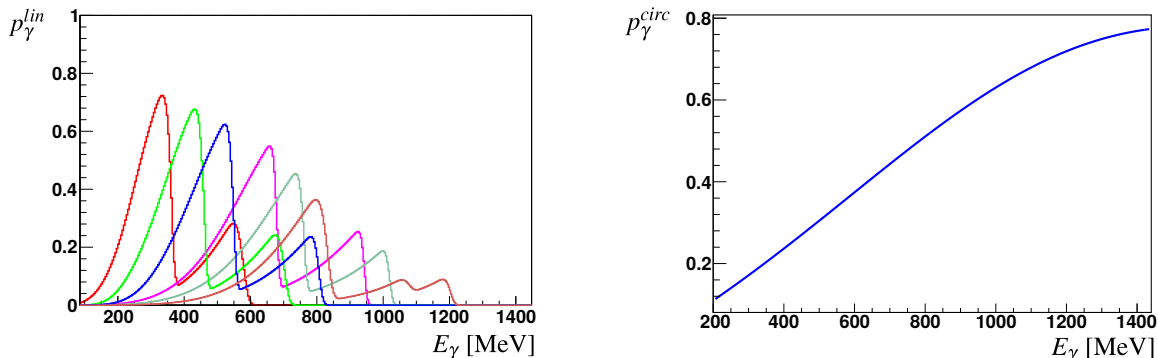


Figure 8: Left: Linear polarization available with a collimator of 2 mm diameter for a variety of crystal orientations. Right: Helicity transfer from the electron to the photon beam as function of the energy transfer. The MAMI beam polarization is $p_e \approx 80\%$. [24]

E_0 (\downarrow) / d_{col} (\rightarrow)	1.5 mm	2.0 mm	2.5 mm	3.0 mm	4.0 mm
180 MeV	0.54	1.0	1.6	2.3	4.2
450 MeV	3.2	5.4	8.3	12.1	19.5
883 MeV	9.9	17.7	25.7	33.1	44.4
1557 MeV	16.0	27.0	37.8	49.0	66.5

Table 4: Tagging efficiencies, in %, for typical incoming electron beam energies (E_0) and photon collimator diameters (d_{col}).

B.2 Frozen-Spin Target

polarization experiments using high density solid-state targets in combination with tagged photon beams can reach the highest luminosities. For the double polarization measurements planned with the Crystal Ball detector on polarised protons and deuterons a specially designed, large horizontal $^3\text{He}/^4\text{He}$ dilution refrigerator was built in cooperation

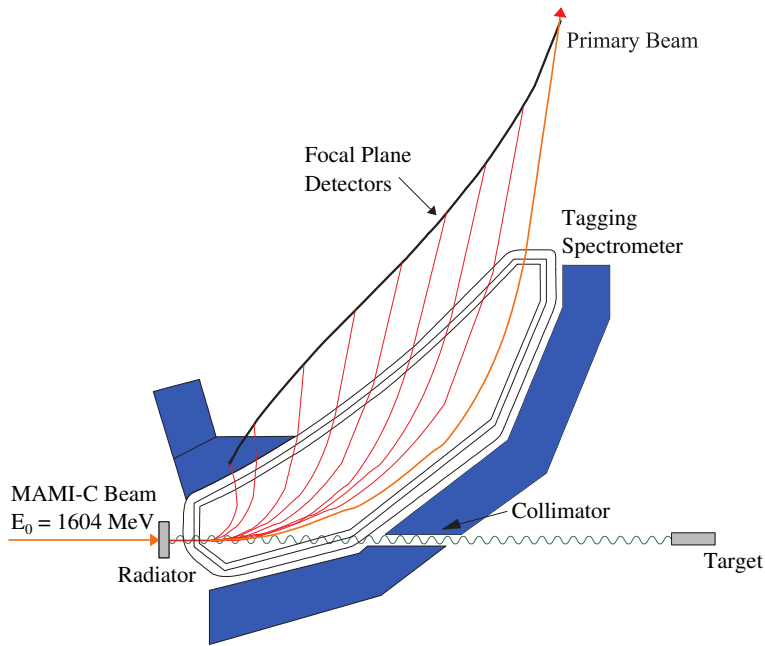


Figure 9: The A2 photon tagging system with the Glasgow-Mainz spectrometer.

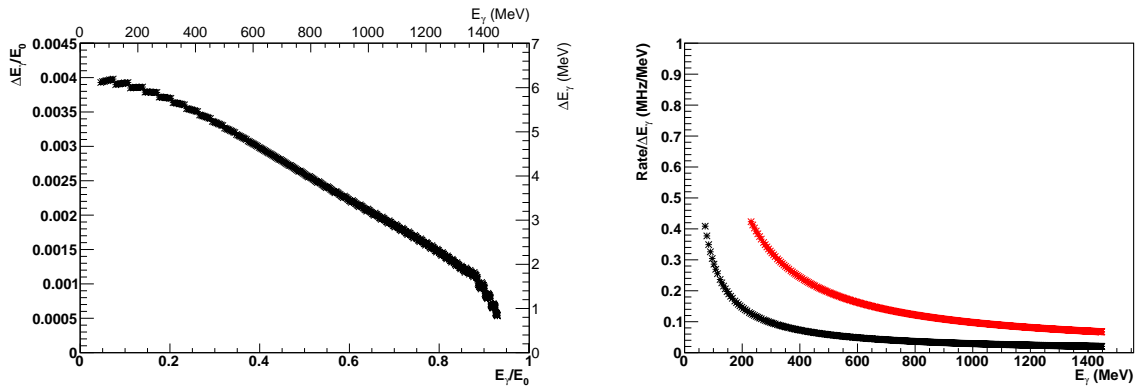


Figure 10: (Left) Tagger channel width (resolution) as a function of the tagged photon energy. The left and bottom axes show these values as relative to the incoming electron beam energy. The right and top axes show these values for a standard electron beam energy of 1557 MeV. (Right) Rates in MHz per MeV for a beam energy of 1557 MeV, assuming a $1/E_\gamma$ Bremsstrahlung distribution, if the first channel is run at 2.5 MHz (black) or if the first 25 channels are switched off and the next is run at 2.5 MHz (red).



Figure 11: The dilution refrigerator for the Crystal Ball Frozen Spin Target.

with the Joint Institute for Nuclear Research (JINR) Dubna (see Fig. 11). It has minimum limitations for the particle detection and fits into the central core of the inner Particle Identification Detector (PID). This was achieved by using the frozen spin technique with the new concept of placing a thin superconducting holding coil inside the polarization refrigerator. Longitudinal and transverse polarizations will be possible.

Highest nucleon polarization in solid-state target materials is obtained by a microwave pumping process, known as ‘Dynamic Nucleon polarization’ (DNP). This process is applicable to any nucleus with spin and has already been used in different experiments with polarised proton and deuteron targets. The geometric configuration of the target is the same for the polarised proton and neutron setup. However, since the polarization measurement of the deuteron is more delicate due to the small size of the polarization signals, the modification of some basic components is needed. The reason for this is twofold: firstly the magnetic moment of the deuteron is smaller than that of the proton and, in addition, the interaction of the deuteron quadrupole moment with the electric field gradient in the sample broadens the deuteron polarization signal. An accuracy $\delta P_p/P_p$ of 2 to 3% for the protons and $\delta P_D/P_D$ of 4 to 5% for the deuterons is expected in the polarization measurement. It has also to be taken into account that the measured deuteron polarization P_D is not equal to the neutron polarization P_n . Assuming a 6 % admixture of the D-state of the deuteron, a calculation based on the Clebsch-Gordon coefficients leads to $P_n = 0.91 P_D$. Several polarised proton and deuteron materials are available such as alcohols and deuterated alcohols (e.g. butanol C_4H_9OH), NH_3 , ND_3 or 6LiD . The most important criteria in the choice of material suitable for particle physics experiments

are the degree of polarization P and the ratio k of free polarisable nucleons to the total number of nucleons. Further requirements on polarised target materials are a short polarization build-up time and a simple, reproducible target preparation. The polarization resistance against radiation damage is not an issue for experiments with a low intensity tagged photon beam ($\dot{N}_\gamma \approx 5 \cdot 10^7 \text{ s}^{-1}$) as will be used here.

Taking all properties together, butanol and deuterated butanol are the best material for this experiment. For protons we expect a maximum polarization of $P_p = 90\%$ and an average polarization of $P_p = 70\%$ in the frozen spin mode. Recently, a deuteron polarization $P_D = 80\%$ was obtained with Trityl doped butanol targets at 2.5 T magnetic field in a $^3\text{He}/^4\text{He}$ dilution refrigerator. At a 0.4 T holding field an average neutron polarization P_n (see above) of 50 % will be obtained. The filling factor for the ~ 2 mm diameter butanol spheres into the 2 cm long, 2 cm diameter target container will be around 60%. The experience from the GDH runs in 1998 [31] shows that, with a total tagged photon flux of $5 \cdot 10^7$, relaxation times of about 1000 hours can be expected. The polarization has to be refreshed by microwave pumping every two days.

In conclusion, we estimate that we will achieve the following target parameters:

- Maximum total tagged photon flux in the energy range of 4.7 to 93% of E_0 : $\dot{N}_\gamma \approx 5 \cdot 10^7 \text{ s}^{-1}$, with relaxation time of 200 hours.
- Target proton density in 2 cm cell: $N_T \approx 9.1 \cdot 10^{22} \text{ cm}^{-2}$ (including dilution and filling factors)
- Average proton polarization $P_p = 70\%$
- Target deuteron density in 2cm cell: $N_T \approx 9.4 \cdot 10^{22} \text{ cm}^{-2}$ (including dilution and filling factors)
- Average neutron polarization $P_n = 50\%$

B.3 Crystal Ball Detector System

The central detector system consists of the Crystal Ball calorimeter combined with a barrel of scintillation counters for particle identification and two coaxial multiwire proportional counters for charged particle tracking. This central system provides position, energy and timing information for both charged and neutral particles in the region between 21° and 159° in the polar angle (θ) and over almost the full azimuthal (ϕ) range. At forward angles, less than 21° , reaction products are detected in the TAPS forward wall. The full, almost hermetic, detector system is shown schematically in Fig. 12 and the measured two-photon invariant mass spectrum is shown in Fig. 13.

The Crystal Ball detector (CB) is a highly segmented 672-element NaI(Tl), self triggering photon spectrometer constructed at SLAC in the 1970's. Each element is a truncated triangular pyramid, 41 cm (15.7 radiation lengths) long. The Crystal Ball has an energy resolution of $\Delta E/E = 0.020 \cdot E[\text{GeV}]^{0.36}$, angular resolutions of $\sigma_\theta = 2 \dots 3^\circ$ and $\sigma_\phi = \sigma_\theta / \sin \theta$ for electromagnetic showers [32]. The readout electronics for the Crystal Ball were completely renewed in 2003, and it now is fully equipped with SADCs which allow for the full sampling of pulse-shape element by element. In normal operation, the onboard summing capacity of these ADCs is used to enable dynamic pedestal subtraction and the provision of pedestal, signal and tail values for each element event-by-event. Each

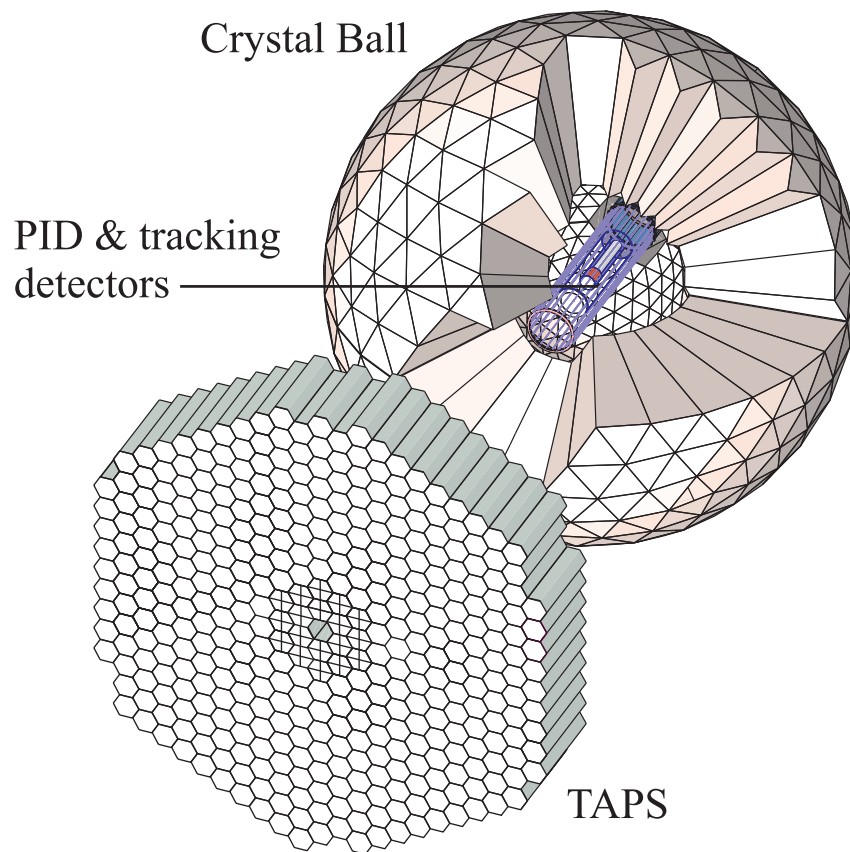


Figure 12: The A2 detector setup: The Crystal Ball calorimeter, with cut-away section showing the inner detectors, and the TAPS forward wall.

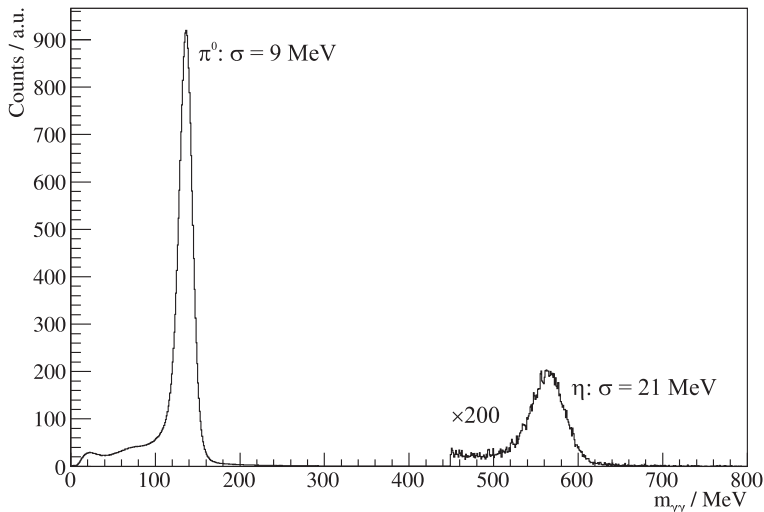


Figure 13: Two photon invariant mass spectrum for the CB/TAPS detector setup. Both η and π^0 mesons can be clearly seen.

CB element is also newly equipped with multi-hit CATCH TDCs. The readout of the CB is effected in such a way as to allow for flexible triggering algorithms. There is an analogue sum of all ADCs, allowing for a total energy trigger, and also an OR of groups of sixteen crystals to allow for a hit-multiplicity second-level trigger - ideal for use when searching for high multiplicity final states.

In order to distinguish between neutral and charged particles species detected by the Crystal Ball, the system is equipped with PID, a barrel detector of twenty-four 50 mm long, 4 mm thick scintillators, arranged so that each PID scintillator subtends an angle of 15° in ϕ . By matching a hit in the PID with a corresponding hit in the CB, it is possible to use the locus of the $\Delta E, E$ combination to identify the particle species (Fig. 14). This is primarily used for the separation of charged pions, electrons and protons. The PID covers from 15° to 159° in θ .

The excellent CB position resolution for photons stems from the fact that a given photon triggers several crystals and the energy-weighted mean of their positions locates the photon position to better than the crystal pitch. For charged particles which deposit their energy over only one or two crystals, this is not so precise. Here the tracks of charged particles emitted within the angular and momentum acceptance of the CB detector will be reconstructed from the coordinates of point of intersections of the tracks with two coaxial cylindrical multiwire proportional chambers (MWPCs) with cathode strip readout. These MWPCs are similar to those installed inside the CB during the first round of MAMI-B runs [33]. The most significant difference is that all detector signals are taken at the upstream end of the MWPCs, minimising the material required and facilitating particle detection in the forward polar region.

A mixture of argon (79.5%), ethane (30%) and freon-CF₄ (0.5%) is used as the filling gas. This mixture is a compromise between charge multiplication and localization requirements imposed by the ionizing particle tracks.

Within each chamber both the azimuthal and the longitudinal coordinates of the avalanche will be evaluated from the centroid of the charge distribution induced on the

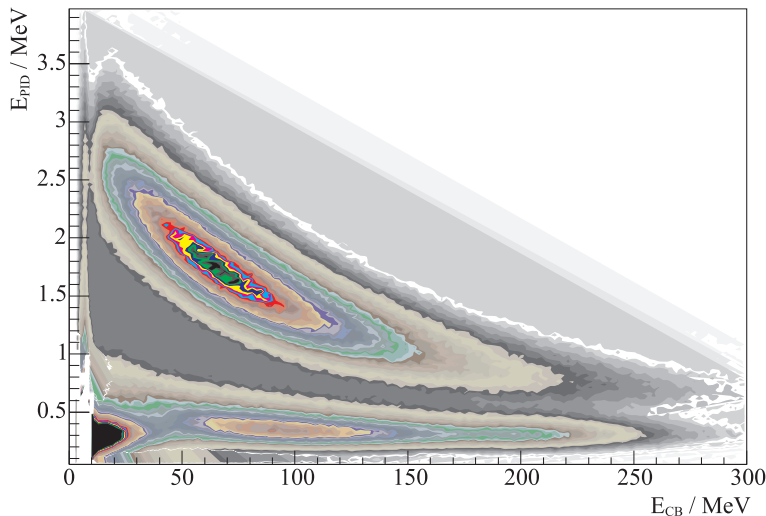


Figure 14: A typical $\Delta E/E$ plot from the Crystal Ball and the PID detector. The upper curved region is the proton locus, the lower region contains the pions and the peak towards the origin contains mostly electrons.

cathode strips. The location of the hit wires(s) will be used to resolve ambiguities which arise from the fact that each pair of inner and outer strip cross each other twice. The expected angular resolution (rms) will be $\sim 2^\circ$ in the polar emission angle θ and $\sim 3^\circ$ in the azimuthal emission angle ϕ .

B.4 TAPS Forward Wall

The TAPS forward wall is composed of 384 BaF_2 elements, each 25 cm in length (12 radiation lengths) and hexagonal in cross section, with a diameter of 59 mm. The front of every TAPS element is covered by a 5 mm thick plastic veto scintillator. The single counter time resolution is $\sigma_t = 0.2$ ns, the energy resolution can be described by $\Delta E/E = 0.018 + 0.008/E[\text{GeV}]^{0.5}$ [32]. The angular resolution in the polar angle is better than 1° , and in the azimuthal angle it improves with increasing θ , being always better than $1/R$ radian, where R is the distance in centimeters from the central point of the TAPS wall surface to the point on the surface where the particle trajectory meets the detector. The TAPS readout was custom built for the beginning of the CB@MAMI program and is effected in such a way as to allow particle identification by Pulse Shape Analysis (PSA), Time Of Flight (TOF) and $\Delta E/E$ methods (using the energy deposit in the plastic scintillator to give ΔE). TAPS can also contribute to the CB multiplicity trigger and is currently divided into upto six sectors for this purpose. The 2 inner rings of 18 BaF_2 elements have been replaced recently by 72 PbWO_4 crystals each 20 cm in length (22 radiation lengths). The higher granularity improves the rate capability as well as the angular resolution. The crystals are operated at room temperature. The energy resolution for photons is similar to BaF_2 under these conditions [34].

C Additional useful information

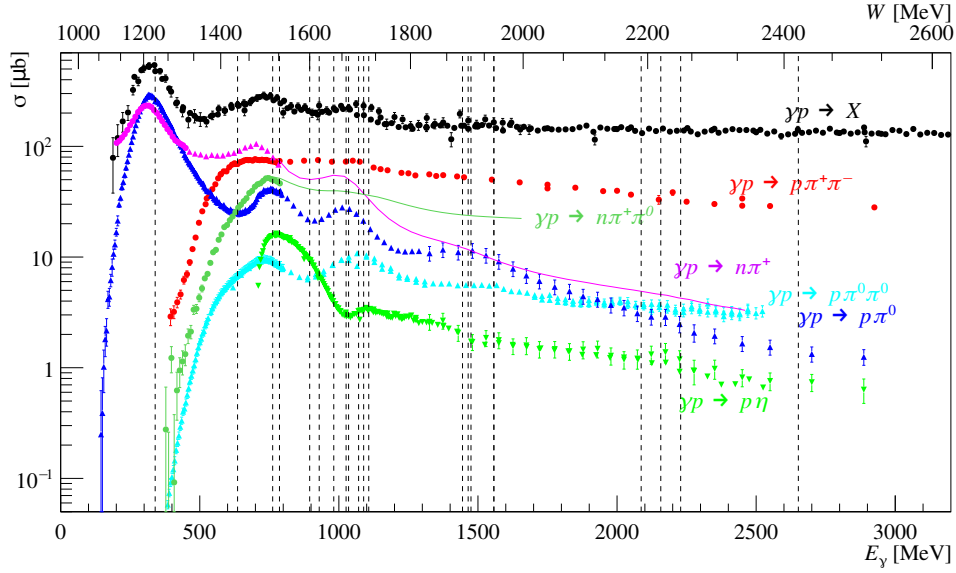


Figure 15: The total cross section is shown for several different final states. [25]

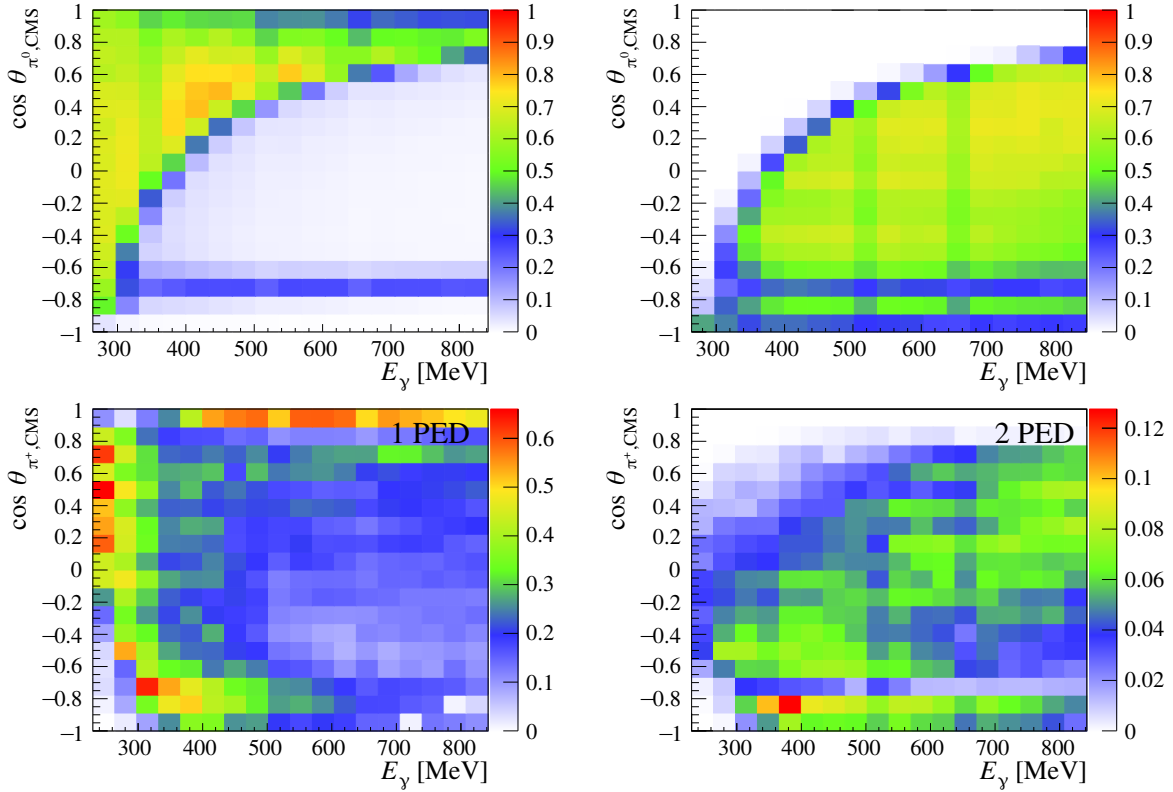


Figure 16: The detection and reconstruction efficiencies are given as a function of the incident photon energy E_γ and $\cos\theta_\pi$ in the upper row for the $p\pi^0$ (right (left): if the proton is (not) detected) and in the bottom row for the $n\pi^+$ final state (right (left): if the neutron is (not) detected) according to Monte Carlo simulations. [25]

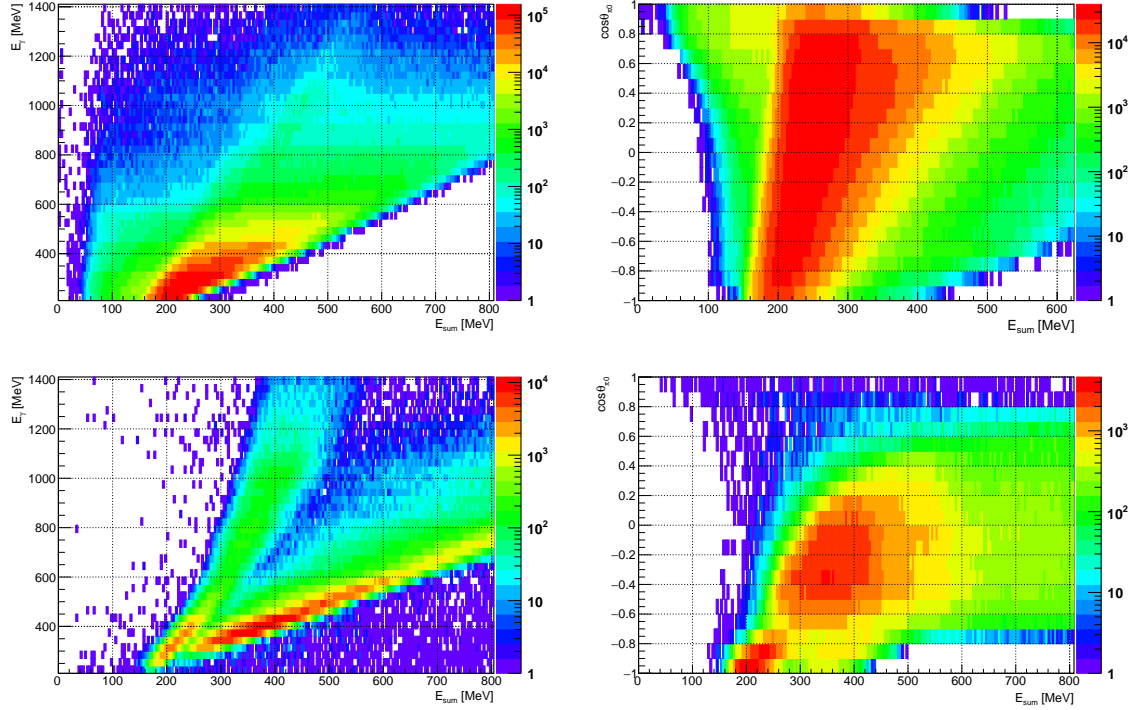


Figure 17: The *CB Esum* (data) is plotted for the $p\pi^0$ final state as a function of the beam photon energy E_γ (left column) and as a function of $\cos\theta_{\pi^0}$ (right column). In the bottom (upper) row the proton is (not) detected.

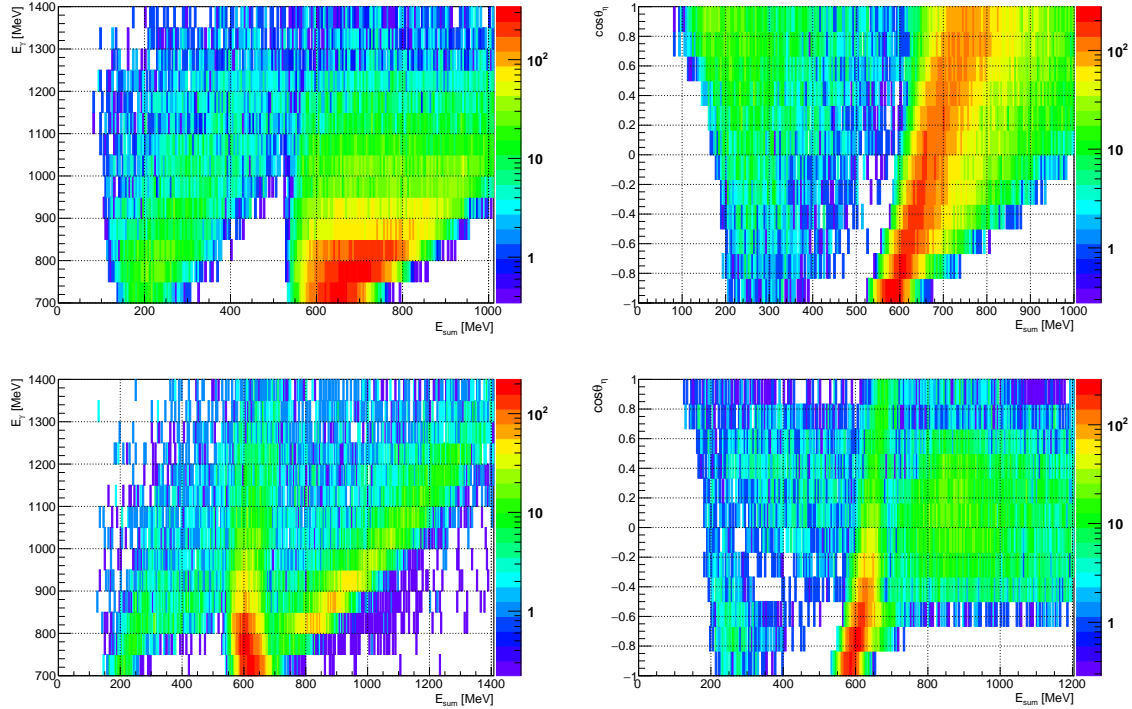


Figure 18: The *CB Esum* (data) is plotted for the $p\eta$ final state as a function of the beam photon energy E_γ (left column) and as a function of $\cos\theta_\eta$ (right column). In the bottom (upper) row the proton is (not) detected.

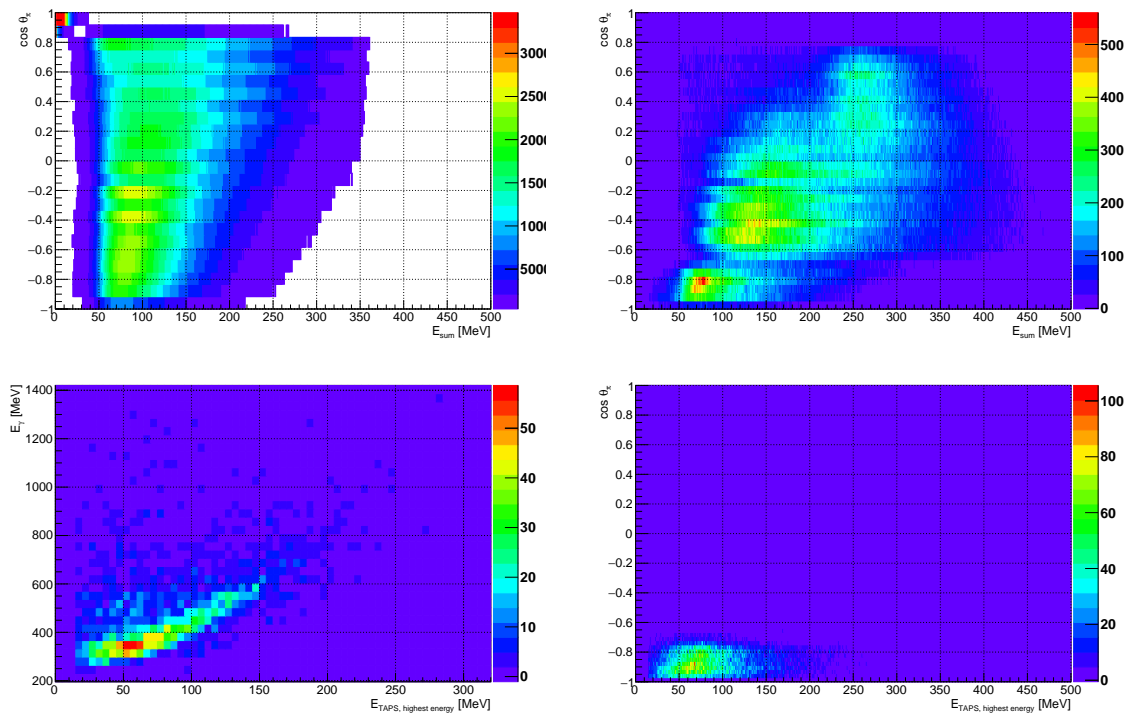


Figure 19: Upper row: The $CB\ Esum$ (data) is plotted for the $n\pi^+$ final state as a function of $\cos\theta_{\pi^+}$ for the case that only the π^+ is detected (left) and for the case that both π^+ and n are detected. In both cases the $CB\ Esum$ trigger will not be able to cover the forward angular range ($\cos\theta_{\pi^+} > 0.7$). Bottom row: The highest deposited energy in one BaF_2 crystal of the TAPS calorimeter (data) is plotted for the $n\pi^+$ final state, once as a function of the beam photon energy (left) and once as a function of $\cos\theta_{\pi^+}$.

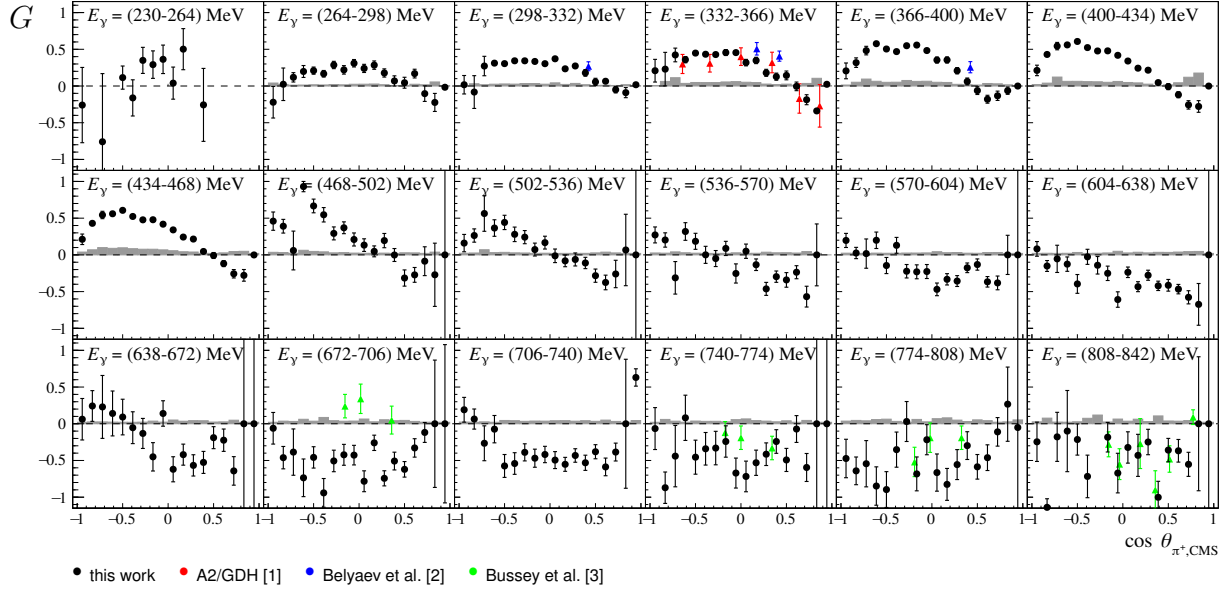


Figure 20: The double polarization observable G is shown as a function of $\cos \theta_{\pi^+}$ for an energy range of $230 \text{ MeV} \leq E_\gamma \leq 842 \text{ MeV}$ for the $n\pi^+$ final state (black points). The data is compared to old GDH data [35] (red points), data of [36] (green points) and of [37] (blue points). Taken from [25].

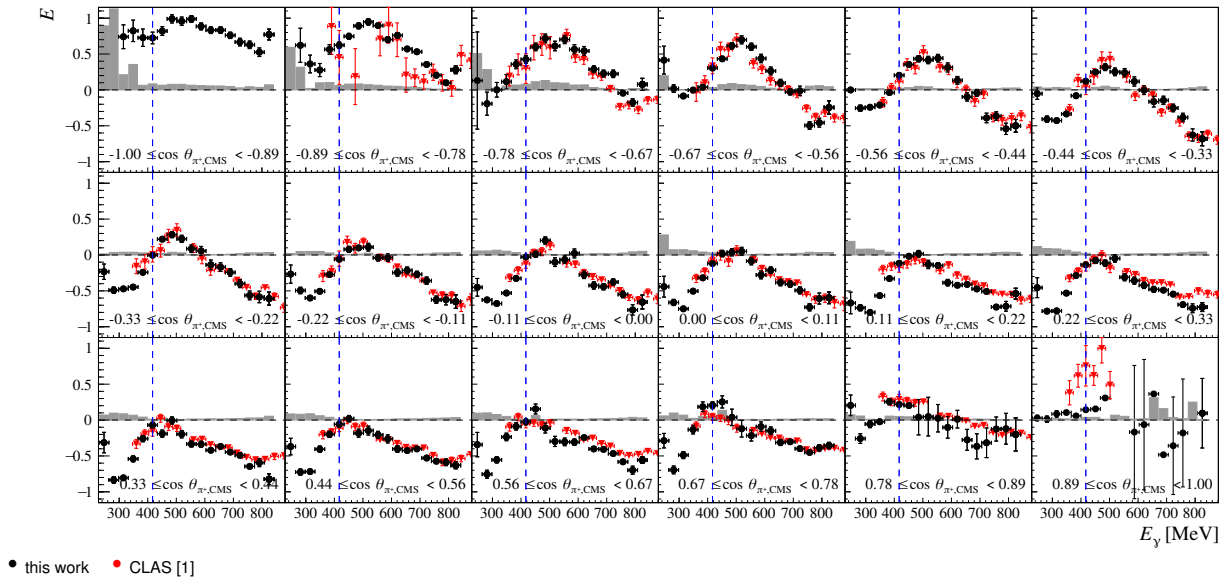


Figure 21: The double polarization observable E is shown as a function of E_γ for all $\cos \theta_{\pi^+}$ bins for the $n\pi^+$ final state (black points). The data is compared to data of the CLAS collaboration (red points) [38]. Taken from [25].

References

- [1] W. T. Chiang and F. Tabakin, Phys. Rev. C **55**, 2054 (1997) doi:10.1103/PhysRevC.55.2054 [nucl-th/9611053].
- [2] K. Nakayama, Phys. Rev. C **100**, no. 3, 035208 (2019) doi:10.1103/PhysRevC.100.035208 [arXiv:1809.00335 [nucl-th]].
- [3] Y. Wunderlich, "The complete experiment problem of pseudoscalar meson photoproduction in a truncated partial wave analysis", url: <http://hss.ulb.uni-bonn.de/2019/5353/5353.htm>, PhD-thesis, University of Bonn (2019).
- [4] V. F. Grushin, in *Photoproduction of Pions on Nucleons and Nuclei*, edited by A. A. Komar (Nova Science, New York, 1989), p. 1ff.
- [5] A. S. Omelaenko, Sov. J. Nucl. Phys. **34**, 406 (1981).
- [6] L. Tiator, private communication (2016).
- [7] A. M. Sandorfi, S. Hoblit, H. Kamano and T.-S. H. Lee, J. Phys. G **38**, 053001 (2011) doi:10.1088/0954-3899/38/5/053001 [arXiv:1010.4555 [nucl-th]].
- [8] Y. Wunderlich, R. Beck and L. Tiator, Phys. Rev. C **85**, 055203 (2014).
- [9] D. Hornidge *et al.* [A2 and CB-TAPS Collaborations], Phys. Rev. Lett. **111**, no. 6, 062004 (2013) doi:10.1103/PhysRevLett.111.062004 [arXiv:1211.5495 [nucl-ex]].
- [10] R. Leukel and R. Beck, *Pion photoproduction results from MAMI*, In D. Drechsel and L. Tiator, editors, proceedings of the NSTAR2000 Conference, page 14 (2001).
- [11] R. Leukel, *Photoproduktion neutraler Pionen am Proton mit linear polarisierten Photonen im Bereich der $\Delta(1232)$ -Resonanz*, PhD-thesis, University of Mainz (2001).
- [12] S. Schumann *et al.* [MAINZ-A2 Collaboration], Phys. Lett. B **750**, 252 (2015). doi:10.1016/j.physletb.2015.09.015
- [13] A. A. Belyaev *et al.*, *Experimental Studies of the Σ , T , P Polarization Parameters and the $\gamma p \rightarrow \pi^0 p$ reaction Multipole Analysis in the first Resonance Region*, Nucl. Phys., B 213:201-222 (1983).
- [14] Y. Wunderlich, F. Afzal, A. Thiel and R. Beck, Eur. Phys. J. A **53**, no. 5, 86 (2017) doi:10.1140/epja/i2017-12255-0 [arXiv:1611.01031 [physics.data-an]].
- [15] R. L. Workman, M. W. Paris, W. J. Briscoe and I. I. Strakovsky, Phys. Rev. C **86**, 015202 (2012) doi:10.1103/PhysRevC.86.015202 [arXiv:1202.0845 [hep-ph]].
- [16] (SAID Partial Wave Analysis) <http://gwdac.phys.gwu.edu/>
- [17] R. Workman, private communication (2015).
- [18] B. Efron and R. J. Tibshirani, *An Introduction to the Bootstrap*, Chapman & Hall/CRC (1994).

- [19] (Bonn-Gatchina Partial Wave Analysis) <http://pwa.hiskp.uni-bonn.de/>
- [20] (MAID Partial Wave Analysis) <http://www.kph.uni-mainz.de/MAID/>
- [21] K. M. Watson, Phys. Rev. **95**, 228 (1954). doi:10.1103/PhysRev.95.228
- [22] H. Osmanovi *et al.*, Phys. Rev. C **100**, no. 5, 055203 (2019) doi:10.1103/PhysRevC.100.055203 [arXiv:1908.05167 [nucl-th]].
- [23] A. Švarc, M. Hadimehmedovi, H. Osmanovi, J. Stahov, L. Tiator and R. L. Workman, Phys. Rev. C **89**, no. 6, 065208 (2014) doi:10.1103/PhysRevC.89.065208 [arXiv:1404.1544 [nucl-th]].
- [24] F.N. Afzal, "Measurement of the beam and helicity asymmetries in the reactions $\gamma p \rightarrow p\pi^0$ and $\gamma p \rightarrow p\eta$ ", url: <http://hss.ulb.uni-bonn.de/2019/5551/5551.htm>, PhD thesis, University of Bonn (2019).
- [25] K.P. Spieker: *Measurement of the double polarization observables G and E in neutral and positive pion photoproduction off the proton*, PhD thesis, University of Bonn (2019).
- [26] M. Bashkanov, private communication (2020).
- [27] Y. Wunderlich, "Studies on a complete experiment for pseudoscalar meson photoproduction", Diploma-thesis, University of Bonn (2012).
- [28] C. S. Akondi *et al.*, *Measurement of the Transverse Target and Beam-Target Asymmetries in η Meson Photoproduction at MAMI*, Phys. Rev. Lett. **113** (2014) 102001
- [29] J. Hartmann, *Measurement of Double Polarization Observables in the Reactions $\gamma p \rightarrow p\pi^0$ and $\gamma p \rightarrow p\eta$ with the Crystal Barrel/TAPS Experiment at ELSA*, PhD thesis, University of Bonn, 2017
- [30] J.C. McGeorge *et al.*: *Upgrade of the Glasgow photon tagging spectrometer for Mainz MAMI-C*, Eur. Phys. J. A **37** (2008) 129.
- [31] A. Thomas *et al.*: *The GDH Experiment at MAMI*, Nucl. Phys. B **79** (1999) 591.
- [32] S. Prakhov *et al.*: *Measurement of the Slope Parameter α for the $\eta \rightarrow 3\pi^0$ decay with the Crystal Ball detector at the Mainz Microtron (MAMI-C)*, Phys. Rev. C **79** (2009) 035204.
- [33] G. Audit *et al.*: *DAPHNE: a large-acceptance tracking detector for the study of photoreactions at intermediate energies*, Nucl. Instr. Meth. A **301** (1991) 473.
- [34] R. Novotny *et al.*: *Scintillators for photon detection at medium energies: A comparative study of BaF-2, CeF-3 and PbWO-4*, Nucl. Instrum. Meth. A **486** (2002) 131.
- [35] J. Ahrens *et al.*, *Measurement of the G asymmetry for the $\gamma p \rightarrow N\pi$ channels in the $\Delta(1232)$ resonance region*, Eur. Phys. J. A **26** (2005) 135.

- [36] P.J. Bussey et al., *Measurement of the polarization parameters G and H in positive photoproduction*, Nucl. Phys. B **403-414** (1980) 83.
- [37] A. Belayev et al., *Investigation of the G and H parameters for the reaction $\gamma p \rightarrow n\pi^+$ in the region of the first πN resonance*, Sov. J. Nucl. Phys. **40** (1984) 83.
- [38] S. Strauch et al.: *First Measurement of the Polarization Observable E in the $\vec{p}(\gamma, \vec{\pi}^+)n$ Reaction up to 2.25 GeV*, Phys. Lett. B **750** (2015) 53-58.